microplate counter (Micro Beta Plus; Wallac, Turku, Finland). ELISAs for human IFN-γ, IL-5, and IL-10 were performed using ELISA kits (OptEIA; BD-Biosciences, Boston, MA, USA) according to the manufacturer's protocols.

Cytotoxicity Assay

To prepare effector cells, cultures with IL-2 and irradiated GM-CSF-transduced autologous tumor cells as described above were prepared in 96-well round-bottomed plates and the plates were cultured for 7 days. On the day of the assay, aliquots of 100 μl of the culture medium were removed from each well and then labeled target cells (5×10^3 cells/100 μl/well) were added. To label the target cells, single-cell suspensions of cultured autologous or allogeneic RCC cells, autologous NRC, and K562 cells were incubated with $Na_2^{51}CrO_4$ (100 μCi) for 1 h at 37°C and washed three times prior to use. For blocking experiments, F(ab′)2 anti-CD3 mAb prepared as described previously [44] was added to a final concentration of 10 μg/ml at the start of the assay. The plates were incubated at 37°C for 6 h, the supernatants were collected using a Skatron cell harvester system (Diversified Equipment Co., Lorton, VA, USA), and the radioactivity was measured using a γ counter. Spontaneous release (SR) and maximal release (MR) were measured in the supernatant of target cells alone with 100 μl of either medium or 10% Triton X-100 (Sigma, St. Louis, MO, USA). The percentage specific cytotoxicity was calculated using the following formula: % cytotoxicity = experimental release − SR/MR − SR × 100.

Analysis of the TCR β Repertoire

Total RNA was isolated from PBMC and homogenized tumor tissues using Trizol reagent (Invitrogen) with a cryo-press crusher (Microtech Nichion, Tokyo, Japan). TCR β repertoire analysis was performed as described previously [45]. Briefly, TCR β cDNA was synthesized using C-oligonucleotides (5′-CGGGCTGCTCCTT GAGGGGCTGCG-3′) with AMV reverse transcriptase (Invitrogen). The TCR cDNA was amplified by 40 cycles of PCR with each of the 24 Vβ 5′ primers (Vβ 1-w24) and the Cβ 3′ primer in PCR buffer containing 1 U of Hot Start *Taq* polymerase (AmpliTaq Gold; Applied Biosystems, Foster City, CA, USA). The products were subjected to Southern blot analysis using a ^{32}P-labeled Cβ probe. Different samples of each Vβ product were compared after quantifying the autoradiographs by densitometry BAS-2000II (Fuji Photo Film Corp.). To refine CDR3 size analysis, the Vβ–Cβ PCR product was copied in a 10-cycle run-off reaction with a fluorescence-labeled Cβ primer. The labeled PCR products were electrophoresed on a DNA sequencer (ABI Prism 377; Applied Biosystems) in the presence of a fluorescent size standard and analyzed with a DNA fragment size program (GeneScan; Applied Biosystems).

The PCR products of the CDR3 fragment were cloned into the pCRII-TOPO vector system (Invitrogen). Thirty colonies containing the insert fragment were selected at random and sequenced using an ABI Prism Cycle Sequencing Kit (Applied Biosystems) and an automatic DNA sequencer ABI 373 (Applied Biosystems). The amino acid sequence of the CDR3 region was deduced using the software GENETYX-MAC v10.1.4 (Software Development Co., Ltd., Tokyo, Japan).

Detection of Antitumor Antibodies

The antitumor antibodies appearing in patients' sera were detected by Western blot analysis according to the standard procedure with some modifications [18]. Briefly, humoral antitumor immune responses were evaluated using the reactivity of the tumor cell lysate and sera from the patients. Autologous RCC and NRC were extracted in lysis buffer containing 20 mM Tris–HCl at pH 7.6, 1% NP-40, 150 mM NaCl, 1 mM phenylmethylsulfonyl fluoride, and 500 units/ml aprotinin (Calbiochem, La Jolla, CA, USA). A fibroblast cell line of human lip origin, which was established in our laboratory, and a small-cell lung carcinoma cell line, H69, were used as irrelevant control cells. Cell lysates were denatured, reduced in SDS sample buffer with 2-mercaptoethanol, and then electrophoresed on 7.5% polyacrylamide minigels (Bio-Rad Laboratories, Hercules, CA, USA). The proteins were transferred onto Immobilon membranes (Millipore, Bedford, MA, USA) and the blots were stained with Ponceau S solution (Sigma) for visualization. After destaining with TBST (0.1% Tween 20–Tris-buffered saline) and blocking with 5% nonfat dried milk in TBST overnight, the blots were probed with diluted (1:300) patient sera for 2 h. Horseradish peroxidase-conjugated rabbit F(ab′)2 anti-IgG Ab (DAKO, 1:3000 dilution) was added for 1 h, and the blots were developed with an ECL kit (Amersham Biosciences, Piscataway, NJ, USA).

ACKNOWLEDGMENTS

We thank Drs. Fumihiko Komine, Tsuyoshi Tanabe, Hitomi Nagayama, Hitoshi Hibino, Muneomi Endo, Tomoko Yamazaki, Mariko Morishita, Koichiro Kuwabara, Momoyo Ohki, Sanae Suzuki, and the staff of The Advanced Clinical Research Center, Research Hospital, The Institute of Medical Science, University of Tokyo, for their excellent patient care and their strong support of this clinical study. We also thank Drs. Ken-ichi Tobisu and Hiroyuki Fujimoto (National Cancer Center, Japan), Taro Shuin (Kochi Medical College), Shunichi Fukuhara (Kyoto University), Yusuke Nakamura (The Institute of Medical Science, University of Tokyo), Toshio Kuroki (Gifu University), Ken-ichi Arai (The Institute of Medical Science, University of Tokyo), Jonathan W. Simons (Emory University), and Glenn Dranoff (Dana-Farber Cancer Institute) for helpful advice and discussions. This work was supported by grants from the Ministry of Health, Labor, and Welfare and the Ministry of Education, Culture, Sports, Science, and Technology, Japan.

RECEIVED FOR PUBLICATION JULY 5, 2004; ACCEPTED JULY 5, 2004.

REFERENCES

1. Marumo, K., *et al.* (2001). The prevalence of renal cell carcinoma: nation-wide survey in Japan in 1997. *Int. J. Urol.* 8: 359–365.
2. Medical Research Council Renal Cancer Collaborators Interferon-α and survival in

doi:10.1016/j.ymthe.2004.07.001

metastatic renal carcinoma: early results of a randomized controlled trial. *Lancet* **353:** 14–17.
3. Bukowski, R. M. (1997). Natural history and therapy of metastatic renal cell carcinoma. *Cancer* **80:** 1198–1220.
4. Motzer, R. J., Bacik, J., Murphy, B. A., Russo, P., and Mazumdar, M. (2002). Interferon-α as a comparative treatment for clinical trials of new theraples against advanced renal cell carcinoma. *J. Clin. Oncol.* **20:** 289–296.
5. Clark, J. I., *et al.* (1999). Daily subcutaneous ultra-low-dose interleukin 2 with daily low-dose interferon-α in patients with advanced renal cell carcinoma. *Clin. Cancer Res.* **5:** 2374–2380.
6. Tagliaferri, P., *et al.* (1998). Daily low-dose subcutaneous recombinant interleukin-2 by alternate weekly administration. *Am. J. Clin. Oncol.* **21:** 48–53.
7. Figlin, R. A., *et al.* (1999). Multicenter, randomized, phase III trial of $CD8^+$ tumor-infiltrating lymphocytes in combination with recombinant interleukin-2 in metastatic renal cell carcinoma. *J. Clin. Oncol.* **17:** 2521–2529.
8. Childs, R., *et al.* (2000). Regression of metastatic renal-cell carcinoma after non-myeloablative allogeneic peripheral-blood stem-cell transplantation. *N. Engl. J. Med.* **343:** 750–758.
9. Dranoff, G., *et al.* (1993). Vaccination with irradiated tumor cells engineered to secrete murine granulocyte-macrophage colony-stimulating factor stimulates potent, specific, and long-lasting anti-tumor immunity. *Proc. Natl. Acad. Sci. USA* **90:** 3539–3543.
10. Jaffee, E. M., Thomas, M. C., Huang, A. Y. C., Hauda, K. M., Levitsky, H. I., and Pardoll, D. M. (1996). Enhanced immune priming with spatial distribution of paracrine cytokine vaccines. *J. Immunother.* **19:** 176–183.
11. Dranoff, G. (2002). GM-CSF-based cancer vaccines. *Immunol. Rev.* **188:** 147–154.
12. Ellem, K. A., *et al.* (1997). A case report: immune responses and clinical course of the first human use of granulocyte/macrophage-colony-stimulating-factor-transduced autologous melanoma cells for immunotherapy. *Cancer Immunol. Immunother.* **44:** 10–20.
13. Berns, A. J., *et al.* (1995). Phase I study of non-replicating autologous tumor cell injections using cells prepared with or without GM-CSF gene transduction in patients with metastatic renal cell carcinoma. *Hum. Gene Ther.* **6:** 347–368.
14. Simons, J. W., *et al.* (1997). Bioactivity of autologous irradiated renal cell carcinoma vaccines generated by ex vivo granulocyte-macrophage colony-stimulating factor gene transfer. *Cancer Res.* **57:** 1537–1546.
15. Simons, J. W., *et al.* (1999). Induction of immunity to prostate cancer antigens: results of a clinical trial of vaccination with irradiated autologous prostate tumor cells engineered to secrete granulocyte-macrophage colony-stimulating factor using ex vivo gene transfer. *Cancer Res.* **59:** 5160–5168.
16. Soiffer, R., *et al.* (1998). Vaccination with irradiated autologous melanoma cells engineered to secrete human granulocyte-macrophage colony-stimulating factor generates potent antitumor immunity in patients with metastatic melanoma. *Proc. Natl. Acad. Sci. USA* **95:** 13141–13146.
17. Chang, A. E., Li, Q., Bishop, D. K., Normolle, D. P., Redman, B. D., and Nickoloff, B. J. (2000). Immunogenic therapy of human melanoma utilizing autologous tumor cells transduced to secrete granulocyte-macrophage colony-stimulating factor. *Hum. Gene Ther.* **11:** 839–850.
18. Jaffee, E. M., *et al.* (2001). Novel allogeneic granulocyte-macrophage colony-stimulating factor-secreting tumor vaccine for pancreatic cancer: a phase I trial of safety and immune activation. *J. Clin. Oncol.* **19:** 145–156.
19. Kusumoto, M., *et al.* (2001). Phase 1 clinical trial of irradiated autologous melanoma cells adenovirally transduced with human GM-CSF gene. *Cancer Immunol. Immunother.* **50:** 373–381.
20. Salgia, R., *et al.* (2003). Vaccination with irradiated autologous tumor cells engineered to secrete granulocyte-macrophage colony-stimulating factor augments antitumor immunity in some patients with metastatic non-small-cell lung carcinoma. *J. Clin. Oncol.* **21:** 624–630.
21. Soiffer, R., *et al.* (2003). Vaccination with irradiated, autologous melanoma cells engineered to secrete granulocyte-macrophage colony-stimulating factor by adeno-viral-mediated gene transfer augments antitumor immunity in patients with metastatic melanoma. *J. Clin. Oncol.* **21:** 3343–3350.
22. Nemunaitis, J., *et al.* (2004). Granulocyte-macrophage colony-stimulating factor gene-modified autologous tumor vaccines in non-small-cell lung cancer. *J. Natl. Cancer Inst.* **96:** 326–331.
23. Tani, K., *et al.* (2000). Progress reports on immune gene therapy for stage IV renal cell carcinoma using lethally irradiated granulocyte-macrophage colony-stimulating factor-transduced autologous renal cancer cells. *Cancer Chemother. Pharmacol.* **46**(Suppl.): S73–S76.
24. Kawai, K., *et al.* (2002). Advanced renal cell carcinoma treated with granulocyte-macrophage colony-stimulating factor gene therapy: a clinical course of the first Japanese experience. *Int. J. Urol.* **9:** 462–466.
25. Thomas, M. C., Greten, T. F., Pardoll, D. M., and Jaffee, E. M. (1998). Enhanced tumor protection by granulocyte-macrophage colony-stimulating factor expression at the site of an allogeneic vaccine. *Hum. Gene Ther.* **9:** 835–843.
26. Borrello, I., Sotomayor, E. M., Cooke, S., and Levitsky, H. I. (1999). A universal granulocyte-macrophage colony-stimulating factor-producing bystander cell line for use in the formation of autologous tumor cell-based vaccines. *Hum. Gene Ther.* **10:** 1983–1991.
27. Luznik, L., *et al.* (2003). Successful therapy of metastatic cancer using tumor vaccines in mixed allogeneic bone marrow chimeras. *Blood* **101:** 1645–1652.
28. Mastrangelo, M. J., *et al.* (1999). Intratumoral recombinant GM-CSF-encoding virus as gene therapy in patients with cutaneous melanoma. *Cancer Gene Ther.* **6:** 409–422.
29. Hanada, K. -I., Yewdell, J. W., and Yang, J. C. (2004). Immune recognition of a human renal cancer antigen through post-translational protein splicing. *Nature* **427:** 252–256.
30. Puisieux, I., *et al.* (1996). Restriction of the T-cell repertoire in tumor-infiltrating lymphocytes from nine patients with renal-cell carcinoma: relevance of the CDR3 length analysis for the identification of in situ clonal T-cell expansions. *Int. J. Cancer* **66:** 201–208.
31. Gaudin, C., *et al.* (1995). In vivo local expansion of clonal T cell subpopulations in renal cell carcinoma. *Cancer Res.* **55:** 685–690.
32. Gaugler, B., *et al.* (1996). A new gene encoding for an antigen recognized by autologous cytolytic T lymphocytes on a human renal carcinoma. *Immunogenetics* **44:** 323–330.
33. Vissers, J. L. M., *et al.* (1999). The renal cell carcinoma-associated antigen G250 encodes a human leukocyte antigen (HLA)-A2.1-restricted epitope recognized by cytotoxic T lymphocytes. *Cancer Res.* **59:** 5554–5559.
34. Rosenberg, S. A., *et al.* (1987). A progress report on the treatment of 157 patients with advanced cancer using lymphokine-activated killer cells and interleukin-2 or high-dose interleukin-2 alone. *N. Engl. J. Med.* **316:** 889–895.
35. Nakazaki, Y., *et al.* (1998). Vaccine effect of granulocyte-macrophage colony-stimulating factor or CD80 gene-transduced murine leukemia/lymphoma cells and their cooperative enhancement of antitumor immunity. *Gene Ther* **5:** 1355–1362.
36. Wang, Z., Qiu, S. J., Ye, S. L., Tang, Z. Y., and Xiao, X. (2001). Combined IL-12 and GM-CSF gene therapy for murine hepatocellular carcinoma. *Cancer Gene Ther.* **8:** 751–758.
37. Van Elsas, A., Hurwitz, A. A., and Allison, J. P. (1999). Combination immunotherapy of B16 melanoma using anti-cytotoxic T lymphocyte-associated antigen 4 (CTLA-4) and granulocyte/macrophage colony-stimulating factor (GM-CSF)-producing vaccines induces rejection of subcutaneous and metastatic tumors accompanied by auto-immune depigmentation. *J. Exp. Med.* **190:** 355–366.
38. Kojima, T., *et al.* (2003). Tumor-derived Gp96 combined with GM-CSF gene-transduced tumor cells inhibit tumor growth in mice through migration and maturation of $CD11c^+$ cells. *Hum. Gene Ther.* **14:** 715–728.
39. Buzio, C., *et al.* (1997). Effectiveness of very low doses of immunotherapy in advanced renal cell cancer. *Br. J. Cancer* **76:** 541–544.
40. Lissoni, P., *et al.* (2002). Ten-year survival results in metastatic renal cell cancer patients treated with monoimmunotherapy with subcutaneous low-dose interleukin-2. *Anticancer Res.* **22:** 1061–1064.
41. Schomburg, A., *et al.* (1992). In vivo and ex vivo antitumor activity in patients receiving low-dose subcutaneous recombinant interleukin-2. *Nat. Immunol.* **11:** 133–143.
42. Sobol, R. E., *et al.* (1999). Interleukin 2 gene therapy of colorectal carcinoma with autologous irradiated tumor cells and genetically engineered fibroblasts: a phase I study. *Clin. Cancer Res.* **5:** 2359–2365.
43. Tani, K., *et al.* (1989). Implantation of fibroblasts transfected with human granulocyte colony-stimulating factor (G-CSF) cDNA into mice as a model of cytokine supplement gene therapy. *Blood* **74:** 1274–1280.
44. Azuma, M., Cayabyab, M., Buck, D., Phillips, J. H., and Lanier, L. L. (1992). CD28 interaction with B7 costimulates primary allogeneic proliferative responses and cytotoxicity mediated by small, resting T lymphocytes. *J. Exp. Med.* **175:** 353–360.
45. Hase, H., *et al.* (2000). Case report: the availability of TCR-Vβ repertoires analysis with RT-PCR methods for the early detection of pulmonary relapsed T-cell malignancy after the autologous stem cell transplantation. *Am. J. Hematol.* **64:** 124–127.

0022-5347/05/1731-0243/0
THE JOURNAL OF UROLOGY®

Vol. 173, 243–246, January 2005
Printed in U.S.A.
DOI: 10.1097/01.ju.0000141577.98902.49

DNA HYPOMETHYLATION ON PERICENTROMERIC SATELLITE REGIONS SIGNIFICANTLY CORRELATES WITH LOSS OF HETEROZYGOSITY ON CHROMOSOME 9 IN UROTHELIAL CARCINOMAS

TOHRU NAKAGAWA, YAE KANAI,* SAORI USHIJIMA, TADAICHI KITAMURA, TADAO KAKIZOE AND SETSUO HIROHASHI

From the Pathology Division, National Cancer Center Research Institute (TN, YK, SU, SH), Department of Urology, Faculty of Medicine, Tokyo University (TN, TKi) and National Cancer Center (TKa), Tokyo, Japan

ABSTRACT

Purpose: DNA methylation has important roles in genomic stability. Accordingly DNA hypomethylation on pericentromeric satellite regions may induce chromosomal instability through heterochromatin decondensation and chromosomal recombination enhancement. We elucidated the significance of aberrant DNA methylation on pericentromeric satellite regions during urothelial carcinogenesis.

Materials and Methods: We examined DNA methylation status on satellites 2 and 3 by Southern blotting and determined the allelic status of chromosome 9 using 6 microsatellite markers (D9S775, D9S925, D9S304, D9S303, D9S283 and D9S747) in 27 transitional cell carcinomas of the bladder, ureter or renal pelvis and corresponding noncancerous tissues.

Results: DNA hypomethylation on satellites 2 and 3 was detected in 2 (7%) and no (0%) noncancerous tissues, and in 11 (41%) and 12 (44%) urothelial carcinomas, respectively. DNA hypomethylation in urothelial carcinomas significantly correlated with histological grade ($p = 0.0012$ and 0.0043), invasion depth ($p = 0.0055$ and 0.0228) and morphological structure (papillary vs nodular, $p = 0.0161$ and 0.0297) for satellites 2 and 3, respectively. Loss of heterozygosity on at least 1 locus of chromosome 9 was detected in 14 urothelial carcinomas (52%). DNA hypomethylation on satellites 2 ($p = 0.0098$) and 3 ($p = 0.0034$) significantly correlated with loss of heterozygosity on chromosome 9.

Conclusions: DNA hypomethylation on pericentromeric satellite regions may participate in the development and progression of urothelial carcinomas by inducing loss of heterozygosity on chromosome 9.

KEY WORDS: urothelium; carcinoma, transitional cell; DNA methylation; chromosomal instability; loss of heterozygosity

DNA methylation has important roles in transcriptional regulation, chromatin remodeling and genomic stability.[1] Satellites 2 and 3, which are related families containing a frequent 5 bp repeat, are abundant in pericentromeric heterochromatin regions on chromosomes 1, 9 and 16, and heavily methylated in normal somatic cells.[2] DNA hypomethylation on such pericentromeric satellite regions may induce chromosomal instability through heterochromatin decondensation and chromosomal recombination enhancement.[3,4] DNA hypomethylation on satellites 2 and 3 has been reported to cause chromosomal instability, such as the formation of multiradiate chromosomes composed of chromosomes 1, 9 and 16, in ICF (immunodeficiency-chromosomal instability-facial anomalies) syndrome.[2]

In human cancers overall DNA hypomethylation accompanied by region specific hypermethylation is generally observed.[1] Aberrant DNA methylation may be involved in carcinogenesis by at least three possible mechanisms: induction of genomic instability as a result of decreased methylation level,[5–7] increased gene mutagenicity caused by deamination of 5-methylcytosine to thymine and repression of gene transcription through CpG island methylation in specific gene regulatory regions, including tumor suppressor genes.[1] For example, frequent chromosomal 1q copy gain with a pericentromeric break point has been reported in hepatocellular carcinomas showing DNA hypomethylation on satellite 2.[8]

The role of DNA hypomethylation in urothelial carcinomas is not fully understood, although aberrant hypermethylation on CpG islands around the promoter region and decreased expression of tumor suppressor genes, such as the *p16* and *E-cadherin* genes, have been reported.[9,10] In addition, loss of heterozygosity (LOH) on chromosome 9 is the most common genetic abnormality in urothelial carcinomas.[11] Consequently we focused on the clinicopathological significance of DNA hypomethylation on pericentromeric satellite regions in urothelial carcinomas and examined whether this hypomethylation is the underlying mechanism for LOH on chromosome 9 during human urothelial carcinogenesis.

Submitted for publication May 20, 2004.
Supported by a Grant-in-Aid for the Second Term Comprehensive 10-Year Strategy for Cancer Control and a Grant-in-Aid for Cancer Research from the Ministry of Health, Labor and Welfare of Japan, and a Research Resident Fellowship from the Foundation for Promotion of Cancer Research in Japan (TN).
* Correspondence: Pathology Division, National Cancer Center Research Institute, 5–1-1 Tsukiji, Chuo-ku, Tokyo 104-0045, Japan (FAX: 81–3-3248–2463; e-mail: ykanai@ncc.go.jp).

MATERIALS AND METHODS

Patients and tissue samples. Paired specimens of primary urothelial carcinoma and corresponding noncancerous tissue were obtained from surgically resected specimens from 27 patients (U1 to U27) treated at National Cancer Center Hospital, Tokyo, Japan. The patients were 22 men and 5 women with a mean age ± SD of 67.6 ± 10.5 years (range 50 to 85).

The primary tumor sites were the bladder, ureter and renal pelvis in 13, 5 and 9 patients, respectively. Based on histological examination 5 (19%), 10 (37%) and 12 (44%) tumors were classified as G1, G2 and G3–4 transitional cell carcinoma, while 11 (41%) and 16 (59%) were superficial (pTa and pT1) and invasive (pT2 to pT4), respectively.[12] Morphologically 21 tumors (78%) were papillary carcinoma and 6 (22%) were nodular carcinoma. Noncancerous specimens were obtained from the urothelium distant from the carcinoma.[13] In cases of widely spreading carcinomas in situ, as diagnosed histopathologically in preoperative biopsy specimens, the muscle layer of the bladder or the renal parenchyma was collected as noncancerous specimens since macroscopic examination cannot necessarily discriminate noncancerous urothelium from carcinoma in situ.

Southern blotting for pericentromeric satellite regions. High molecular weight DNA was isolated from fresh tissue samples by phenol-chloroform extraction and dialysis. DNA methylation status was assessed by digesting DNA with *Msp* I and *Hpa* II, which cut at the sequence CCGG. *Hpa* II does not cut when the internal cytosine is methylated. High molecular weight DNA (5 μg) was digested for 24 hours with 10 U *Msp* I or *Hpa* II/μg DNA. DNA fragments were separated by electrophoresis, transferred to nitrocellulose membranes and hybridized with ^{32}P labeled DNA probes. Previously described oligonucleotides were used as probes for satellites 2 and 3.[14]

Analysis of LOH on chromosome 9. Genomic DNA was amplified by polymerase chain reaction (PCR) using oligonucleotide primers for 6 microsatellite loci on chromosome 9, namely D9S775, D9S925, D9S304, D9S303, D9S283 and D9S747. Primer sequences were D9S775 (9p23) 5′-AAAGTAGCCATCCGTGTGT-3′ and 5′-GCTTTCTTTGATGGTTTACAG-3′, D9S925 (9p21–22) 5′-GTCTGGGTTCTCCAAAGAAA-3′ and 5′-TGTGAGCCAAGGCCTTATAG-3′, D9S304 (9p21) 5′-GTGCACCTCTACACCCAGAC-3′ and 5′-TGTGCCCACACACATCTATC-3′, D9S303 (9q21) 5′-CAACAAAGCAAGATCCCTTC-3′ and 5′-TAGGTACTTGGAAACTCTTGGC-3′, D9S283 (9q22) 5′-TGCTGGATTTCAGGTAGGG-3′ and 5′-ATGGTTATGCGGGTGTATTTCTC-3′, and D9S747 (9q32) 5′-GCCATTATTGACTCTGGAAAAGAC-3′ and 5′-CAGGCTCTCAAAATATGAACAAAAT-3′. The 5′ ends of forward primers were labeled with 6-carboxyfluorescein and PCR amplifications were performed with 20 ng genomic DNA. Subsequently PCR products were fractionated by electrophoresis (ABI 3100 sequencer, Applied Biosystems, Foster City, California) according to the manufacturer protocol. Data were analyzed with the GeneScan, version 3.7 computer program (Applied Biosystems). When 2 amplified bands per locus were detected in the noncancerous tissue specimen, the case was considered informative for LOH analysis. LOH was recorded when signal intensity for a tumor allele was decreased by more than 50% relative to the matched normal allele in informative cases, as described previously.[15–17] Replication error was identified by the presence of band shifts or the presence of novel bands in PCR products.

Statistics. Correlations between any 2 of DNA methylation status, allelic status and clinicopathological parameters were analyzed by the chi-square test with $p < 0.05$ considered significant.

RESULTS

DNA methylation status on pericentromeric satellite regions and its correlation with clinicopathological parameters. Figure 1 shows examples of Southern blotting. In 25 (93%) and all 27 (100%) noncancerous tissue specimens examined significantly larger DNA fragments were detected in *Hpa* II digests compared with *Msp* I digests at satellites 2 and 3, respectively, indicating that these regions were heavily methylated. In 11 (41%) and 12 (44%) urothelial carcinomas smaller fragments were detected in *Hpa* II digest compared with corresponding normal tissues or *Hpa* II digest showed almost the same hybridization pattern as the *Msp* I digest of the same sample and the corresponding normal tissue, indicating that these regions were hypomethylated. In almost all carcinoma samples in which DNA hypomethylation was detected hypomethylation occurred on satellites 2 and 3.

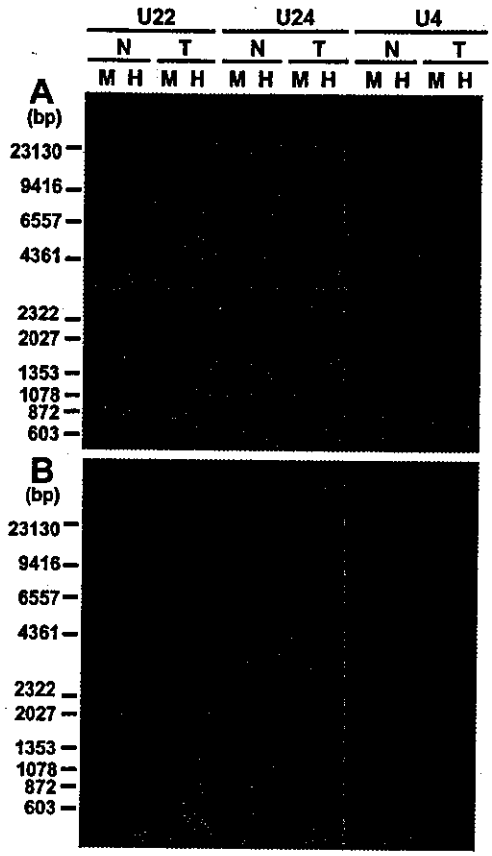

FIG. 1. Examples of Southern blotting for satellites 2 (*A*) and 3 (*B*) in cases of urothelial carcinoma. Methylation status was assessed by digesting DNA with *Msp* I (*Lane M*) and *Hpa* II (*Lane H*). DNA fragments were separated by electrophoresis, transferred to nitrocellulose membranes and hybridized with ^{32}P labeled DNA probes. Larger bands were detected in lane H compared with lane M in all noncancerous tissue (*N*), and in U22T and U24T, indicating that satellite 2 region was heavily methylated (*A*). In U4T lane H showed same hybridization pattern as lane M, indicating that this region was hypomethylated. (*B*) In all noncancerous tissues, and U22T and U24T satellite 3 region was heavily methylated, whereas this region was hypomethylated in U4T. *T*, cancerous tissue.

DNA hypomethylation on pericentromeric satellite regions significantly correlated with histological grade (chi-square test $p = 0.0012$ and 0.0043), invasion depth (chi-square test $p = 0.0055$ and 0.0228) and morphological structure (papillary vs nodular chi-square test $p = 0.0161$ and 0.0297) for satellites 2 and 3, respectively (table 1), but not with age or gender (data not shown).

Allelic status of chromosome 9 and its correlation with clinicopathological parameters. Figure 2 shows examples of electropherograms of PCR products. Figure 3 shows the results of LOH analysis. Table 2 lists the incidence of LOH on each locus. LOH for at least 1 marker was found in 14 of the 27 informative cases (52%) (table 2).

The presence of LOH on at least 1 locus on chromosome 9 significantly correlated with histological grade (chi-square test $p = 0.0313$, table 3). LOH on at least 1 locus was detected in all 6 nodular carcinomas and its incidence (100%) was significantly higher than in papillary carcinomas (chi-square test $p = 0.0074$, table 3).

Correlation between DNA methylation status on pericentromeric satellite regions and allelic status of chromosome 9. DNA

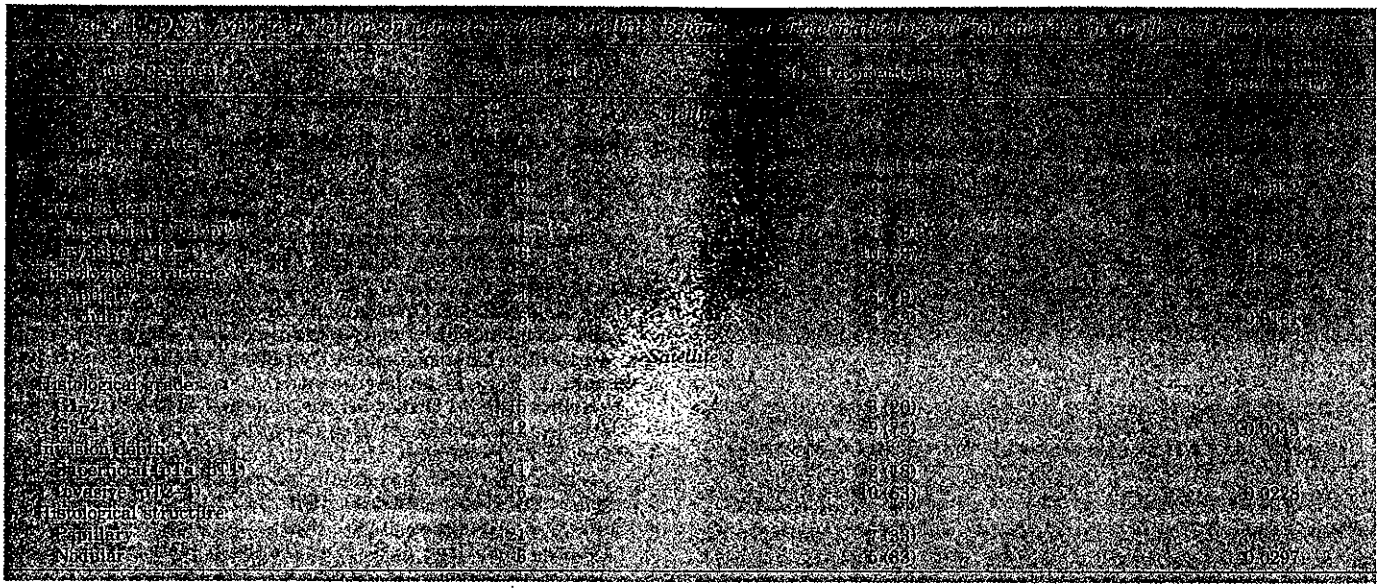

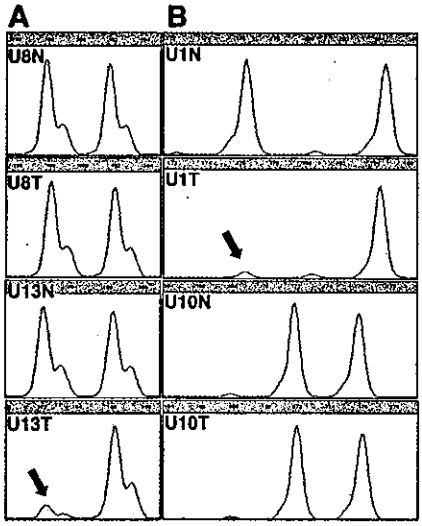

FIG. 2. Examples of results of allelic status analyses in cases of urothelial carcinoma. U8 and U13 DNA samples were amplified for D9S747 (*A*), while U1 and U10 samples were amplified for D9S775 (*B*). Genotypes derived from noncancerous U8N, U13N, U1N and U10N tissues, and corresponding U8T, U13T, U1T and U10T cancerous tissues are shown. Allele size in bp is indicated on top of horizontal axis. In all 4 noncancerous samples PCR products showed polymorphism, indicating that these cases were informative. U8T for D9S747 and U10T for D9S775 were classified as retention of alleles because signal intensity for tumor alleles was not changed significantly relative to matched normal alleles. LOH was identified when signal intensity for tumor allele was decreased by more than 50% relative to matched normal allele, that is in U13T for D9S747 and U1T for D9S775 (arrows).

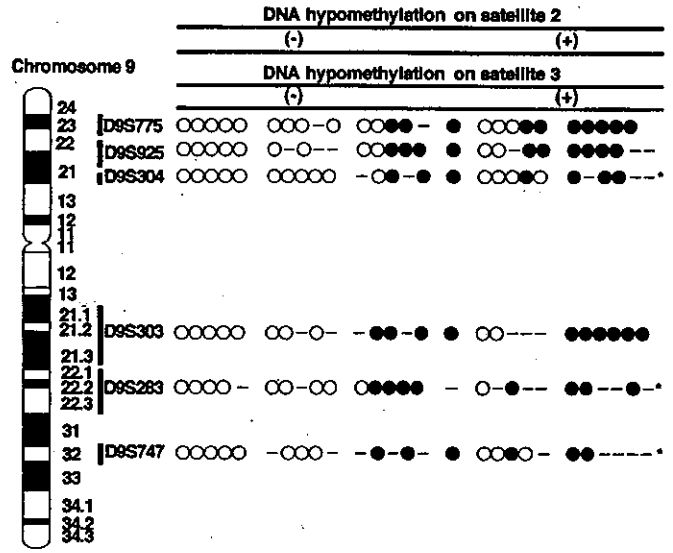

FIG. 3. Allelic status of each locus in urothelial carcinomas. Vertical lines indicate each carcinoma. Open circles indicate retention of 2 alleles. Filled circle indicate LOH. Bar indicates uninformative case. Asterisk indicates replication error. −, negative. +, positive.

TABLE 2. *LOH on chromosome 9 in urothelial carcinomas*

Locus	No. Analyzed	No. Informative	% LOH (%)
9p			
D9S775	27	23	13 (42)
D9S925	27	21	10 (48)
D9S304	27	22	7 (32)
Any on 9p	27	26	11 (42)
9q			
D9S303	27	20	10 (50)
D9S283	27	18	8 (44)
D9S747	27	17	6 (35)
Any on 9q	27	26	12 (46)
Any on chromosome 9	27	27	14 (52)

hypomethylation on pericentromeric satellite regions significantly correlated with the presence of LOH on at least 1 locus on chromosome 9 in urothelial carcinomas (chi-square test p = 0.0098 and 0.0034 for satellites 2 and 3, respectively, table 4).

DISCUSSION

DNA hypomethylation on satellites 2 and 3 was observed frequently in urothelial carcinomas but it was extremely rare in noncancerous tissues, suggesting that DNA hypomethylation on satellites 2 and 3 is associated with urothelial carcinogenesis. We have previously reported that DNA hypomethylation on satellites 2 and 3 is a frequent and early event during hepatocarcinogenesis,[18] whereas it is rare in colorectal and stomach cancers.[19] These and the current findings suggest that DNA hypomethylation on pericentromeric satellite regions is organ specific during human carcinogenesis. In the current study DNA hypomethylation correlated with tumor aggressiveness (eg histological grade and invasion depth), indicating that it may participate in the malignant progression of urothelial carcinomas. In addition, DNA hy-

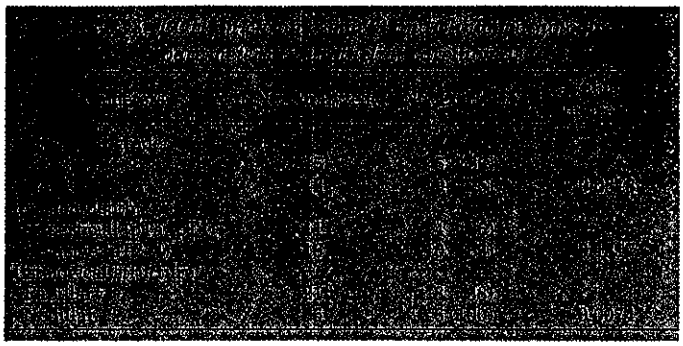

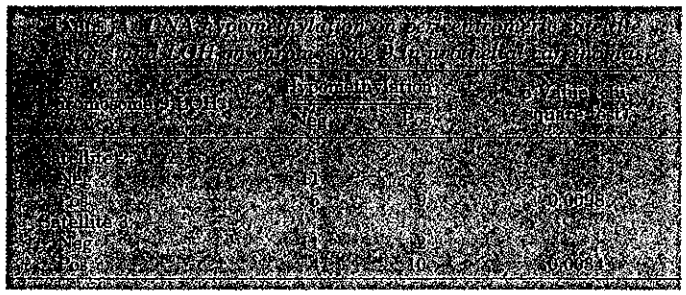

pomethylation was associated more frequently with nodular invasive carcinomas showing an aggressive clinical outcome than with papillary carcinomas. Nodular invasive carcinomas arise from their precursor lesions, that is widely spreading flat carcinoma in situ, and rapidly invading suburothelial tissues, whereas papillary carcinomas usually remain noninvasive for a long period, even after recurrence in the bladder following cystoscopic resection.[13]

LOH on chromosome 9 was detected in more than half of the cases and in these cases rather large regions of 9p and/or 9q were lost, consistent with other reports that loss of an entire chromosome arm is frequent (fig. 3).[11] The observed high incidence of LOH on chromosome 9 in urothelial carcinomas may indicate the existence of tumor suppressor genes important for urothelial carcinogenesis on this chromosome.[11] DNA hypomethylation on satellites 2 and 3 significantly correlated with LOH on chromosome 9 in urothelial carcinomas. After the induction of DNA hypomethylation in cultured cells by treatment with 5-azacytidine, a DNA methyltransferase inhibitor, chromosomal recombination occurred between satellite regions.[3] In patients with ICF syndrome DNA hypomethylation on satellites 2 and 3, and multiradiate chromosomes composed of chromosomes 1, 9 and 16 are characteristic.[2] During hepatocarcinogenesis DNA hypomethylation on satellite 2 significantly correlates with chromosome 1 q-arm copy gain with pericentromeric break points.[8] By analogy with these findings DNA hypomethylation on satellites 2 and 3 could be the underlying molecular background for the frequently observed LOH on chromosome 9 in urothelial carcinomas.

DNMT3b has been identified as a DNA methyltransferase specifically targeting satellites 2 and 3 during mouse development.[20] In human hepatocarcinogenesis over expression of DNMT3b4, a splice variant of DNMT3b that lacks methyltransferase activity and competes with the major variant in normal liver tissues, DNMT3b3, for targeting to pericentromeric satellite regions, results in DNA hypomethylation on these regions.[21] Although further studies are needed to understand the molecular mechanism causing DNA hypomethylation on satellites 2 and 3 during urothelial carcinogenesis, this hypomethylation may have a role in the development and progression of urothelial carcinomas by inducing chromosomal instability. These data highlight the practical significance of correction of DNA methylation status for the prevention and/or therapy of urothelial carcinomas.

REFERENCES

1. Jones, P. A. and Baylin, S. B.: The fundamental role of epigenetic events in cancer. Nat Rev Genet, **3:** 415, 2002
2. Xu, G. L., Bestor, T. H., Bourc'his, D., Hsieh, C. L., Tommerup, N., Bugge, M. et al: Chromosome instability and immunodeficiency syndrome caused by mutations in a DNA methyltransferase gene. Nature, **402:** 187, 1999
3. Kokalj-Vokac, N., Almeida, A., Viegas-Pequignot, E., Jeanpierre, M., Malfoy, B. and Dutrillaux, B.: Specific induction of uncoiling and recombination by azacytidine in classical satellite-containing constitutive heterochromatin. Cytogenet Cell Genet, **63:** 11, 1993
4. Suzuki, T., Fujii, M. and Ayusawa, D.: Demethylation of classical satellite 2 and 3 DNA with chromosomal instability in senescent human fibroblasts. Exp Gerontol, **37:** 1005, 2002
5. Chen, R. Z., Pettersson, U., Beard, C., Jackson-Grusby, L. and Jaenisch, R.: DNA hypomethylation leads to elevated mutation rates. Nature, **395:** 89, 1998
6. Gaudet, F., Hodgson, J. G., Eden, A., Jackson-Grusby, L., Dausman, J., Gray, J. W. et al: Induction of tumors in mice by genomic hypomethylation. Science, **300:** 489, 2003
7. Eden, A., Gaudet, F., Waghmare, A. and Jaenisch, R.: Chromosomal instability and tumors promoted by DNA hypomethylation. Science, **300:** 455, 2003
8. Wong, N., Lam, W. C., Lai, P. B., Pang, E., Lau, W. Y. and Johnson, P. J.: Hypomethylation of chromosome 1 heterochromatin DNA correlates with q-arm copy gain in human hepatocellular carcinoma. Am J Pathol, **159:** 465, 2001
9. Maruyama, R., Toyooka, S., Toyooka, K. O., Harada, K., Virmani, A. K., Zochbauer-Muller, S. et al: Aberrant promoter methylation profile of bladder cancer and its relationship to clinicopathological features. Cancer Res, **61:** 8659, 2001
10. Bornman, D. M., Mathew, S., Alsruhe, J., Herman, J. G. and Gabrielson, E.: Methylation of the E-cadherin gene in bladder neoplasia and in normal urothelial epithelium from elderly individuals. Am J Pathol, **159:** 831, 2001
11. Knowles, M. A.: The genetics of transitional cell carcinoma: progress and potential clinical application. BJU Int, **84:** 412, 1999
12. Sobin, L. H. and Wittekind, Ch.: TNM Classification of Malignant Tumors, 5th ed. New York: John Wiley & Sons, Inc., 1997
13. Friedell, G. H., Parija, G. C., Nagy, G. K. and Soto, E. A.: The pathology of human bladder cancer. Cancer, **45:** 1823, 1980
14. Tagarro, I., Fernandez-Peralta, A. M. and Gonzalez-Aguilera, J. J.: Chromosomal localization of human satellites 2 and 3 by a FISH method using oligonucleotides as probes. Hum Genet, **93:** 383, 1994
15. Hartmann, A., Rosner, U., Schlake, G., Dietmaier, W., Zaak, D., Hofstaedter, F. et al: Clonality and genetic divergence in multifocal low-grade superficial urothelial carcinoma as determined by chromosome 9 and p53 deletion analysis. Lab Invest, **80:** 709, 2000
16. Hartmann, A., Schlake, G., Zaak, D., Hungerhuber, E., Hofstetter, A., Hofstaedter, F. et al: Occurrence of chromosome 9 and p53 alterations in multifocal dysplasia and carcinoma in situ of human urinary bladder. Cancer Res, **62:** 809, 2002
17. Obermann, E. C., Junker, K., Stoehr, R., Dietmaier, W., Zaak, D., Schubert, J. et al: Frequent genetic alterations in flat urothelial hyperplasias and concomitant papillary bladder cancer as detected by CGH, LOH, and FISH analyses. J Pathol, **199:** 50, 2003
18. Saito, Y., Kanai, Y., Sakamoto, M., Saito, H., Ishii, H. and Hirohashi, S.: Expression of mRNA for DNA methyltransferases and methyl-CpG-binding proteins and DNA methylation status on CpG islands and pericentromeric satellite regions during human hepatocarcinogenesis. Hepatology, **33:** 561, 2001
19. Kanai, Y., Ushijima, S., Kondo, Y., Nakanishi, Y. and Hirohashi, S.: DNA methyltransferase expression and DNA methylation of CPG islands and peri-centromeric satellite regions in human colorectal and stomach cancers. Int J Cancer, **91:** 205, 2001
20. Okano, M., Bell, D. W., Haber, D. A. and Li, E.: DNA methyltransferases Dnmt3a and Dnmt3b are essential for de novo methylation and mammalian development. Cell, **99:** 247, 1999
21. Saito, Y., Kanai, Y., Sakamoto, M., Saito, H., Ishii, H. and Hirohashi, S.: Overexpression of a splice variant of DNA methyltransferase 3b, DNMT3b4, associated with DNA hypomethylation on pericentromeric satellite regions during human hepatocarcinogenesis. Proc Natl Acad Sci USA, **99:** 10060, 2002

Reprinted from
Jpn J Clin Oncol 2004;34(3)118–123

Magnetic Anchor for More Effective Endoscopic Mucosal Resection

Toshiaki Kobayashi[1], Takushi Gotohda[1], Katsunori Tamakawa[2], Hirohisa Ueda[3] and Tadao Kakizoe[1]

[1]National Cancer Center, Tokyo, [2]Tamakawa Corporation, Sendai, [3]Pentax Corporation, Tokyo, Japan

Jpn J Clin Oncol 2004;34(3)118–123

Magnetic Anchor for More Effective Endoscopic Mucosal Resection

Toshiaki Kobayashi[1], Takushi Gotohda[1], Katsunori Tamakawa[2], Hirohisa Ueda[3] and Tadao Kakizoe[1]

[1]National Cancer Center, Tokyo, [2]Tamakawa Corporation, Sendai, [3]Pentax Corporation, Tokyo, Japan

Received September 24, 2003; accepted January 16, 2004

Background: Technical difficulties are involved in endoscopic mucosal resection (EMR) of gastric cancer since it is a 'one handed surgery'. These difficulties prevent this technique from being indicated for larger lesions, even when it can possibly be performed for patients with such lesions. If microforceps could assist EMR, this procedure would become easier and safer. Since magnetic force can control objects without direct contact, it can be applied to control microforceps internally in assistance with EMR.
Methods: We developed a magnetic anchor consisting of three parts: a magnetic weight with dimensions of 1.0 × 1.0 × 1.5 cm, microforceps and a connecting thread. Endoscopic clips used in hemostasis were used as the microforceps of the magnetic anchor in this study. The magnetic control system consisted of a 0.68 kOe/10 cm/100 A electromagnet, 350 mm in diameter and a circumventing positional frame. The microforceps were inserted into a sheath within the endoscope, and the magnetic weight was secured to the tip of the sheath protruding from the endoscope. The magnetic anchor, along with the endoscope, was inserted through an overtube into the gastric cavity of a swine under general anesthesia. The magnetic anchor was used in a manner similar to that in standard surgery, and EMR was thereby performed.
Results: The mucosa to be resected was satisfactorily dragged and stabilized. The magnetic anchor facilitated EMR, regardless of the technical skills of the endoscopist and region of the stomach at which the technique was performed.
Conclusion: The magnetic anchor is considered to have alleviated some technical problems involved in EMR. It has the potential for making EMR a safer and quicker procedure for the treatment of early gastric cancer, when appropriately indicated.

Key words: endoscopic mucosal resection (EMR) – microforceps – magnetic anchor – gastric cancer – endoscopic surgery

INTRODUCTION

Endoscopic mucosal resection (EMR) of gastric cancer is a representative procedure of minimally invasive surgery (1). While this approach seems theoretically appropriate, it has serious problems especially when its indications are extended to lesions larger than those recommended by the Japanese Gastric Cancer Association (2). These problems arise from the fact that all resection procedures are carried out using only one endoscope. Thus, resection is performed without appropriate tissue tension provided by an assistant holding the tip of the mucosa. This 'one handed surgery' is the root cause of several problems, particularly when performing EMR on large lesions.

In EMR, the resection line cannot be fully observed because the ablated mucosa cannot be stabilized and pulled up. Consequently, it is difficult to make an accurate incision into the mucosa. Cutting of unconfirmed blood vessels causes bleeding, and hemostatic procedures are hindered because the bleeding point cannot be confirmed directly by operator's eyes. It is also of consequence that the depth of the mucosa at the site of ablation cannot be confirmed, which may lead to perforation of the gastric wall (1,3). These dilemmas have not caused serious problems so far, because EMR is indicated only for relatively small lesions.

Several new techniques and types of equipment have been developed to overcome these technical difficulties and complications that are problematic even for experienced endoscopists. The insulation-tipped electro-surgical knife (IT knife) is one such device that was designed by covering the tip of the electric knife with a ceramic ball to prevent accidental penetration of the gastric wall (1,4).

The rationale behind this development is that the tip of the electric knife, which is the most penetrative part for surgical incision, cannot be used. Thus, theoretically, resection is limited to a certain extent and the penetration is prevented.

For reprints and all correspondence: Toshiaki Kobayashi, Cancer Screening Technology Division, Research Center for Cancer Prevention and Screening, National Cancer Center, 1-1, Tsukiji 5-chome, Chuo-ku, Tokyo 104-0045, Japan. E-mail: tkobayas@ncc.go.jp

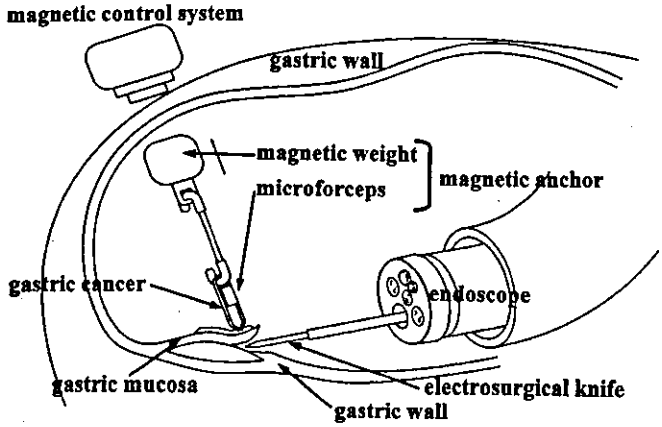

Figure 1. The concept of the magnetic anchor. The concept of the magnetic anchor is shown by microforceps that stabilize and pull up objects by employing a magnetic field. The magnetic anchor consists of three parts: microforceps, a magnetic weight and the connecting thread between them. One application of this concept is the use of the forceps to assist endoscopic resection of gastric cancer. The concept can even be applied to other procedures outside medical practice when stabilization and traction of objects are required and where direct contact is not possible.

However, perforation is still encountered, leading to prolonged resection time. Therefore, EMR for gastric cancer requires an endoscopist with technical skills higher than those required for other endoscopic procedures.

A basic technical principle of surgical resection is the resection of appropriate tissues, which are made to stand out by pulling them up. If this basic technique is integrated into EMR, then the procedure would become easier, less risky and more effective. This, in turn, could make it possible to establish EMR as the standard procedure whenever the nature of the lesions is an indication for resection with EMR, irrespective of their size.

Magnets and magnetic fields have been applied to catheter examinations to control the tips of catheters for years (5). They may also be providing a way to alter tissue contour configurations without any direct contact, such as through electric cables. A direct current magnetic field, as is used in MRI, is regarded as the least invasive, or even the most appropriate, non-invasive procedure that can be applied medically.

If a magnetic field is properly controlled and made to generate enough power to give sufficient force by using microforceps for stabilization of the mucosa during EMR (Fig. 1), then the procedure would be made much easier. If such a device design is developed, then indications for EMR could be expanded to change the current concept of endoscopic surgery for cancer treatment, including gastric cancer.

Thus, this study was initiated to evaluate the potential of magnetically controlled forceps and a magnetic anchor in an animal subject.

a. Positioning frame

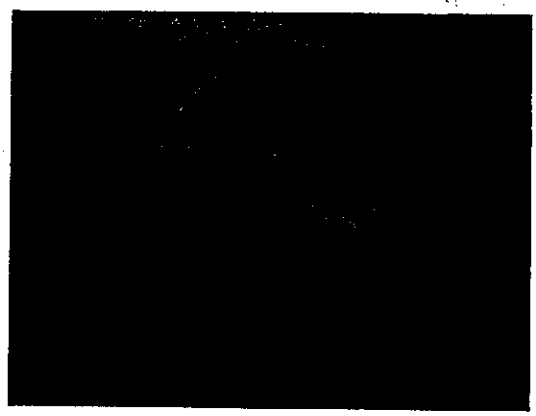

b. Electromagnet fixed to the belts

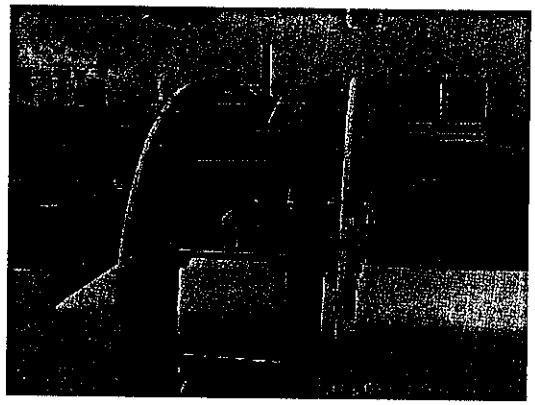

Figure 2. Magnetic control system. (a) Positioning frame: The positioning frame holds the electromagnet and allows its movement around the subject. Its wheels allow lateral movement along the table. (b) Electromagnet fixed to the belts: The electromagnet, shown by the arrow, is fixed to the belts that allow its movement around a subject inside the system. The electromagnet itself is compact; however, the frame is produced on a large scale to keep the distance between the subject and the electromagnet at a minimum.

SUBJECTS AND METHODS

MAGNETIC CONTROL SYSTEM

A magnetic control system was designed for clinical application in a standard endoscopic room, thus limiting the size of the system. The magnetic control system primarily consisted of a 0.68 kOe /100 A electromagnet, 350 mm in diameter, at 10 cm from the center of the magnetic yoke.

The electromagnet was fixed on belts contained in a semicircular positioning frame that revolved around the trails of the frame. In this manner, a pulley system was formed allowing a 180° control of the magnet's position in relation to the patient (Fig. 2).

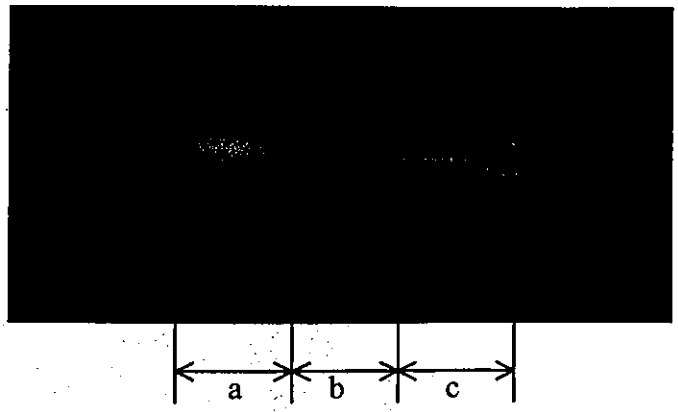

Figure 3. Magnetic anchor. The magnetic anchor consists of three parts: (a) a magnetic weight, (c) microforceps and (b) a thread connecting them.

MAGNETIC ANCHOR

The magnetic anchor consists of three parts: a hand-made magnetic weight comprising magnetic stainless steel (SUS420F), microforceps and a connecting thread (Fig. 3). The weight, with dimensions of 1.0 × 1.0 × 1.5 cm, was designed to generate sufficient traction for tissues and to allow insertion into the gastric cavity through the esophagus. The weight of the anchor can be varied by using differently shaped weight components of different weights. The anchor weight used for this procedure is approximately 6 g.

Hemostasis clips (endo-clips) were used as microforceps in order to confirm the feasibility of the magnetic anchor's proposed function of tissue traction. However, it is likely that forceps designed specially for this procedure will be developed in the future.

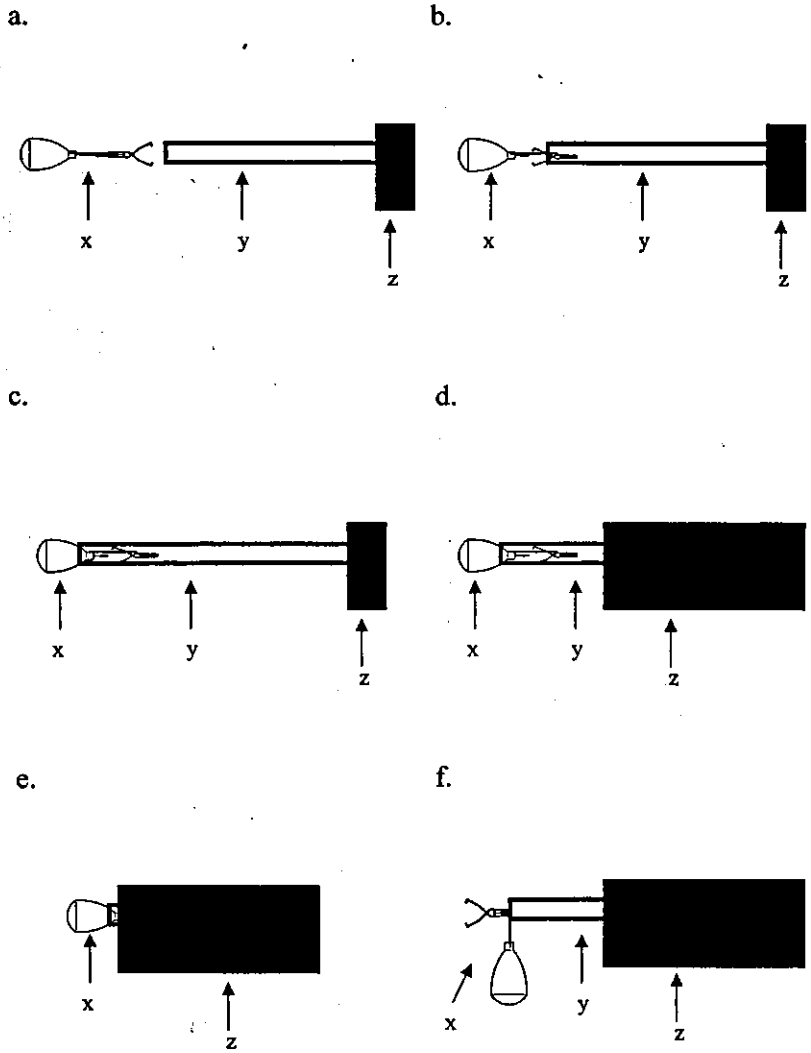

Figure 4. Preparation of the magnetic anchor. (a) The magnetic anchor (x) is prepared by the following procedure: First, the endoscopic hemostasis sheath (y) is inserted into the working channel of an endoscope (z) and pushed out from the tip of the endoscope. (b) The microforceps are connected to the sheath and pulled backwards into the sheath. (c) The thread is pulled further into the sheath together with the magnetic weight, and the magnetic weight is secured at the tip of the sheath. (d) The sheath is pulled into the endoscope. (e) The weight is fixed at the tip of the endoscope. (f) The magnetic anchor is pushed out from the tip of the endoscope at the time of its use. The target is grasped after opening the microforceps. x: magnetic anchor, y: endoscopic hemostasis sheath, z: endoscope.

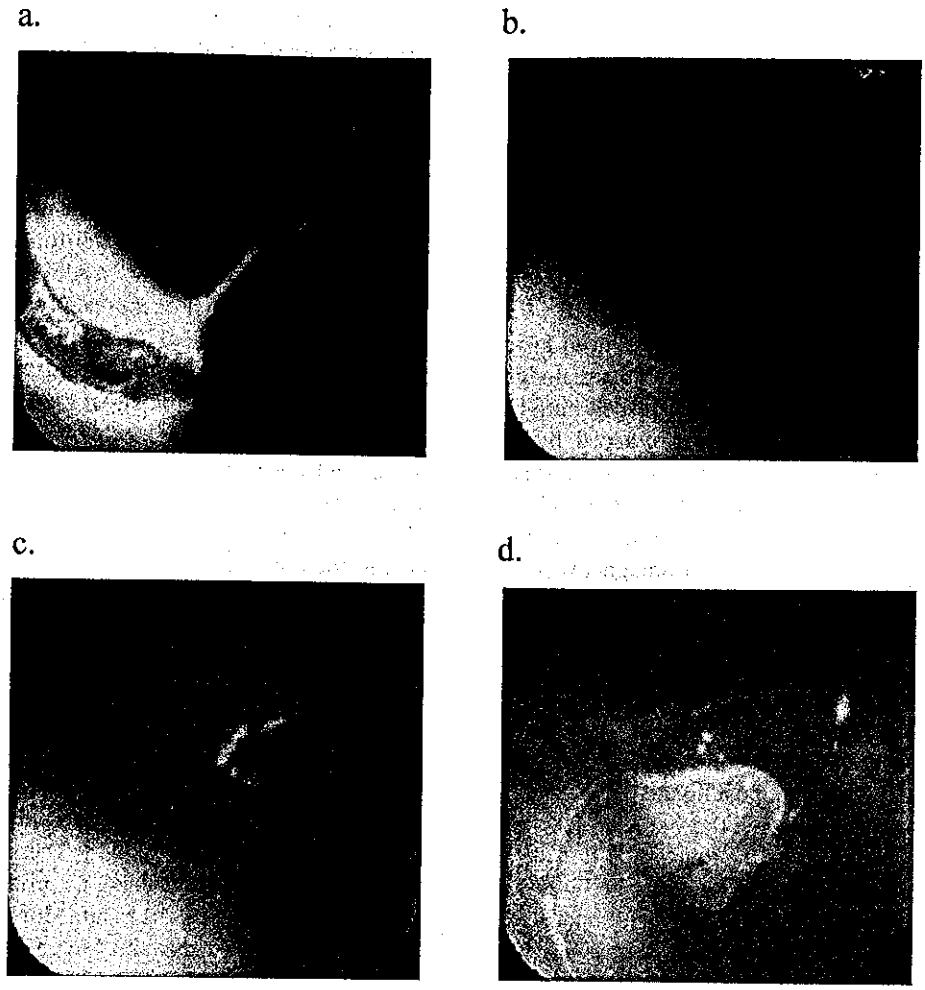

Figure 5. Resection using the magnetic anchor. (a) The mucosa is pulled to create sufficient space to show the line of resection. (b) The resection is performed using an electric knife through an endoscope. (c) The resection line can be clearly shown as a result of traction by the magnetic anchor. (d) The traction of the magnetic anchor is sufficient to allow the mucosal flap to be turned over.

Preparation of the Magnetic Anchor

First, the endoscopic hemostasis sheath is inserted into the working channel of an endoscope as shown in Fig. 4. The microforceps are then connected to the sheath and are pulled backwards into the tip of the sheath protruding from the tip of the endoscope; subsequently, the thread follows and the anchor is secured at the tip of the sheath. The sheath is then withdrawn into the working channel, and the anchor is fixed at the tip of the endoscope.

Test Subject

A 45 kg female swine laid in the left lateral position, was placed on an examination table under intravenous anesthesia.

Procedure

Prior to insertion of the magnetic anchor, an incision was made by the standard EMR technique in the mucosa surrounding the region of the stomach intended for resection (4). An overtube was first inserted into the esophagus to facilitate smooth insertion of the endoscope along with the magnetic anchor to reach the gastric cavity. Inside the gastric lumen, the magnetic weight was pushed out from the sheath, followed by the microforceps. The tip of the mucosa, in which the incision was made in advance, was grasped by the microforceps. In order to lift the tip of the mucosa, a magnetic field was then generated by increasing the electric current through the electromagnet of the magnetic control system.

The EMR procedure was performed by several physicians of the National Cancer Center Hospital at four representative regions of the stomach: the anterior wall of the gastric angle, the lesser curvature of the gastric corpus, the posterior wall of the gastric angle and the greater curvature of the gastric corpus. These areas were selected in order to represent the varying techniques and problems that are incurred with the anatomy of each specific area.

RESULTS

Insertion of the fixed magnetic anchor through the overtube incurred no difficulties. In fact, the magnetic anchor was easily

Table 1. Sizes of resected specimens and the procedure times required

Site in the stomach	Size (cm)	Time (min)
Anterior wall of the gastric angle	5.1 × 2.7	51
Lesser curvature of the gastric corpus	2.4 × 1.7	47
Posterior wall of the gastric angle	2.9 × 1.7	25
Greater curvature of the gastric corpus	9.4 × 5.1	73

introduced even without the overtube. Once introduced inside the gastric lumen, the magnetic weight smoothly dislodged from the sheath and the forceps were easily pushed out. The mucosal target site for traction was easily grasped by the microforceps in the same manner as in endoscopic hemostasis, despite the heaviness of the weight component of the anchor.

As a result of magnetic attraction, the magnetic anchor rose rapidly when the electric current of the electromagnet was sufficient for the operation, pulling up the mucosa in a stable tent-like form (Fig. 5). The direction of the traction for the magnetic anchor could be controlled simply by changing the position of the electromagnet over the animal. Application of magnetic attraction only from above was sufficient to pull the magnetic anchor in the desired direction. The control of the magnetic anchor could also be facilitated by adjusting the position of the swine and/or placing a spacer between the swine and the bed. Thus, the magnetic anchor pulled up the mucosa sufficiently to show the resection line. Moreover, hemorrhage was rare because blood vessels could be clearly visualized endoscopically, and electrocoagulation hemostatic procedures were conducted before cutting the blood vessels. Even on occasions of unexpected hemorrhage, hemostasis proved easier because the site of bleeding was clearly visible by stretching the mucosal folds using the magnetic anchor.

The basic features and functions of the magnetic anchor were similar at all the four tested representative areas of the stomach, and the magnetic anchor could be controlled in the same manner at all sites. Sizes of resected specimens and the procedure time required for each are shown in Table 1.

DISCUSSION

Conventional surgery for cancer is highly stressful and sometimes burdensome for patients. Standard treatment for gastric cancer at present is gastrectomy, which is performed even for early gastric cancer. One alternative to gastrectomy that has recently emerged is EMR, although it has several technical problems related to its one handed surgery approach. This procedure, in turn, demands additional skills that are beyond those required for a standard endoscopic technique.

However, the magnetic anchor is not a technique in itself but just an additional tool which is optionally used by the endoscopist during EMR. In the present experiment, endoscopists used the magnetic anchor throughout the procedure and found that EMR was much easier by using it. This opinion was unanimous even on their first exposure to the new device. The magnetic anchor facilitated resection even with the techniques used for standard EMR, which are different from those used for standard surgery. It is worth noting that it was not necessary for the endoscopists to modify their technique in using the magnetic anchor. In fact, they found that the use of the anchor offered more benefits.

The first EMR procedure using the magnetic anchor was performed by a senior physician, the following two by resident physicians, and the last one by a senior physician with a resident physician. All the procedures were performed with few or no incidents regardless of the skills of the physicians. The senior physician, who has developed skills for using the IT knife, had to modify technique he used for standard surgery in order to maximize the efficacy of the magnetic anchor. However, he did not find it difficult. Even for resident physicians inexperienced with an IT knife, EMR with the magnetic anchor proved easy to perform. According to the endoscopists, one touch to the mucosa made it sufficient for cutting. This was a great contrast to the frustration that they had when performing standard EMR without the magnetic anchor, which demanded much effort and patience.

However, several noteworthy incidents had occurred during the procedure. Prominent among them were separation of the magnetic weight from the thread connecting the forceps and slipping of the microforceps from the mucosa. In these cases, new magnetic anchors could be inserted without any problems, and the procedure was continued. The malfunctioned anchors could be easily removed causing no problem, even when left in the gastric lumen during the resumed resection procedure with a new anchor. Slipping of the forceps occurred twice for the same physician at the same mucosal site. Thus, this may be attributed to his inexperience in surgical techniques, which would be similar to the problems encountered with some assistants in standard surgery. Of greater importance was the unproblematic retrieval of the dislodged magnetic anchor. In fact, one of the reasons for involving various physicians in this experiment was to evaluate the nature of incidents with the device and to consider possible countermeasures for future improvement. Thus, the magnetic anchor will certainly be improved, and refined, and will present with few benign problems that we expect to overcome easily. We emphasize that the magnetic anchors used in this study were merely handmade ones devised to experimentally assess the conceptual feasibility of the technique.

Problems with standard EMR such as perforation and incomplete resection are serious and potentially hinder the EMR procedure from being indicated to lesions proposed for resection by the National Cancer Center Hospital of Japan. Even though indications for EMR procedures may be discussed in later papers, we believe that several current problems with EMR are solved to a great extent by the use of the magnetic anchor.

The results of this study showed that all procedures were satisfactorily performed using an electric current of less than 50 A for the electromagnet, which is comparable to 0.6 kOe/10 cm. Consequently, the intensity of the magnetic field required for

the magnetic anchor for EMR was less than what had been expected prior to this procedure. Our next model of the magnetic control system will be smaller and simpler. New concepts of magnetic anchor will expand the indications of endoscopic surgery beyond the treatment of gastric cancer.

Acknowledgments

This study was supported by a Grant-in-Aid for the Research on Advanced Medical Technology of the Ministry of Health, Labor and Welfare, and a Grant-in-Aid for the Second Term Comprehensive 10-year Strategy for Cancer Control, of the Ministry of Health, Labor and Welfare. The authors thank Professor J. Patrick Barron of the International Medical Communication Center, Tokyo Medical University, for his review of the manuscript, and Professor Ken-ichi Arai of Tohoku University for his technical advice.

References

1. Rembacken BJ, Gotoda T, Fujii T, Axon ATR. Endoscopic mucosal resection. *Endoscopy* 2001;33(8):709–18.
2. Gotoda T, Yanagisawa A, Sasako M, Ono H, Nakanishi Y, Shimoda T, et al. Incidence of lymph node metastasis from early gastric cancer: estimation with a large number of cases at two large centers. *Gastric Cancer* 2000;3:219–25.
3. Tada M. One piece resection and piecemeal resection of early gastric cancer by strip biopsy. *Igakushoin* 1998;68–87 (in Japanese).
4. Gotoda T, Kondo H, Ono H, Saito Y, Yamaguchi H, Saito D, et al. A new endoscopic mucosal resection procedure using an insulation-tipped electrosurgical knife for rectal flat lesions: report of two cases. *Gastrointest Endosc* 1999;50:560–3.
5. Faddis MN, Blume W, Finney J, Hall A, Rauch J, Sell J, et al. Novel, magnetically guided catheter for endocardial mapping and radiofrequency catheter ablation. *Circulation* 2002;106:2980–5.

Fluorine 18–tagged fluorodeoxyglucose positron emission tomographic scanning to predict lymph node metastasis, invasiveness, or both, in clinical T1 N0 M0 lung adenocarcinoma

Hiroaki Nomori, MD, PhD[a]
Kenichi Watanabe, MD[a]
Takashi Ohtsuka, MD[a]
Tsuguo Naruke, MD, PhD[a]
Keiichi Suemasu, MD, PhD[a]
Toshiaki Kobayashi, MD, PhD[b]
Kimiichi Uno, MD, PhD[c]

See related editorial on page 341.

Objective: We sought to predict lymph node metastasis and tumor invasiveness in clinical T1 N0 M0 lung adenocarcinomas, and we measured fluorodeoxyglucose uptake on positron emission tomography.

Methods: Fluorodeoxyglucose positron emission tomography was performed on 44 patients with adenocarcinomas of 1 to 3 cm in size clinically staged as T1 N0 M0 before major lung resection with lymph node dissection. Fluorodeoxyglucose uptake was evaluated by using the contrast ratio between the tumor and contralateral healthy lung tissue. Lymphatic and vascular invasion within tumors, pleural involvement, and grade of histologic differentiation were examined.

Results: The pathologic tumor stage was T1 N0 M0 in 36 patients, and a more advanced stage was found in 8 patients. Although all 22 adenocarcinomas with a contrast ratio of less than 0.5 in fluorodeoxyglucose uptake were pathologic T1 N0 M0 tumors, 8 (36%) of 22 with a contrast ratio of 0.5 or greater were of a more advanced stage than T1 N0 M0, with the difference being significant ($P = .002$). Adenocarcinomas with a contrast ratio of less than 0.5 showed less lymphatic and vascular invasion and less pleural involvement than those with a contrast ratio of 0.5 or greater ($P = .006$, $P = .004$, and $P = .02$, respectively). The grade of histologic differentiation was well differentiated in 19 of 22 adenocarcinomas with a contrast ratio of less than 0.5 (86%), which was a greater frequency than the 4 (18%) of 22 adenocarcinomas with a contrast ratio of 0.5 or greater ($P < .001$).

Conclusion: Clinical T1 N0 M0 lung adenocarcinomas with a contrast ratio of less than 0.5 usually did not have lymph node metastasis, had less tumor involvement of vessels or pleura, and were more frequently well differentiated than those with a contrast ratio of 0.5 or greater. Limited lung resection could be indicated, lymph node dissection or mediastinoscopy could be reduced, or both in this type of adenocarcinoma.

From the Department of Thoracic Surgery,[a] Saiseikai Central Hospital, Tokyo, Japan; the Endoscopy Division,[b] National Cancer Center Hospital, Tokyo, Japan; and Nishidai Clinic,[c] Tokyo, Japan.

This work was supported in part by a Grant-in-Aid from the Ministry of Health, Labor, and Welfare of Japan.

Received for publication Dec 17, 2003; revisions requested Feb 12, 2004; accepted for publication March 22, 2004.

Address for reprints: Hiroaki Nomori, MD, PhD, Department of Thoracic Surgery, Saiseikai Central Hospital, 1-4-17 Mita, Minato-ku, Tokyo 108-0073, Japan (E-mail: hnomori@qk9.so-net.ne.jp).

J Thorac Cardiovasc Surg 2004;128: 396-401

0022-5223/$30.00

doi:10.1016/j.jtcvs.2004.03.020

Recent advances in low-dose helical computed tomography (CT) and video-assisted thoracoscopic surgery have enabled the diagnosis of lung cancers while still small in size.[1-6] Although limited resection procedures, such as lung wedge resection or segmentectomy, can cure some clinical T1 N0 M0 non–small cell lung cancers (NSCLCs),[7,8] lymph node metastases are still found in approximately 20% of clinical T1 N0 M0 lung adenocarcinomas.[9-11] Even for patients with pathologic T1 N0 M0 NSCLCs, tumor involvement of intratumoral vessels or the pleura can also cause local recurrence after limited resection because of the spread of tumor cells into lymphatic vessels outside the primary tumor. To predict which T1 N0 M0 lung adenocarcinomas are curable with limited resection from CT findings, several reports have evaluated the importance of ground-glass opacity (GGO) within tumors, usually indicating bronchioloalveolar carcinoma–like spread because adenocarcinomas with GGO appearance are more frequently N0 stage and have less tumor involvement of intratumoral vessels or pleura than those with a solid appearance.[12,13] The criteria of defining GGO appearance on CT scans are subjective, however, potentially leading to erroneous selection of limited surgical intervention.

In recent years, fluorodeoxyglucose (FDG) positron emission tomography (PET) has been used to evaluate pulmonary nodules and tumor stages. It has been reported that FDG uptake correlates with the proliferative activity of tumors[14,15] and is an independent prognostic factor,[16,17] particularly in lung adenocarcinoma. The prognosis in lung adenocarcinoma is known to depend on not only tumor stage but also tumor involvement of intratumoral vessels or pleura.[9,10,18] To predict lymph node metastases and tumor involvement of intratumoral vessels or pleura in clinical T1 N0 M0 lung adenocarcinomas, we measured FDG uptake to determine any correlation with lymph node metastases, lymphatic and vascular invasion, and pleural involvement.

Materials and Methods

Patients

From December 2001 through October 2003, prospective FDG-PET and CT scans were performed for 223 noncalcified pulmonary nodules. Of these, 93 nodules were malignant tumors less than 3 cm in diameter on CT. Clinical TNM stage was determined by using both CT and PET scanning. Of the 93 malignant nodules, 48 were clinical T1 N0 M0 adenocarcinomas of the lung, and these underwent major lung resection with mediastinal lymph node dissection. We excluded 4 adenocarcinomas less than 1 cm in diameter that were PET negative because the spatial resolution of the current generation of PET scanners is 0.7 to 0.8 cm, making it difficult to image pulmonary nodules of less than 1 cm. As a result, we studied 44 adenocarcinomas that were clinically staged as T1 N0 M0 of sizes from 1 to 3 cm. The medical record of each patient was examined with regard to age, sex, maximum tumor diameter, serum level of carcinoembryonic antigen (CEA; <5 ng/mL vs ≥5 ng/mL), operative procedure, pathologic TNM stage, vascular or lymphatic invasion within tumors (positive vs negative), pleural involvement (p0 vs p1 to p3), and grade of histologic differentiation. To identify tumor involvement of the intratumoral vessels or pleura, we routinely conducted elastica-van Gieson staining. Pleural involvement was classified as p0, p1, p2, or p3; that is, a p0 tumor did not extend beyond the elastic pleural layer, a p1 tumor invaded the visceral pleural elastic layer but did not reach the pleural surface, a p2 tumor included tumor exposure on the pleural surface, and a p3 tumor invaded the parietal pleura or chest wall. The tumor stages were based on the TNM classification of the International Union Against Cancer[19]: p2 tumors were classified as T2; p3 tumors were classified as T3; and tumors with intrapulmonary metastasis within the same lobe were classified as T4. Grades of histologic differentiation were classified as well, moderately, or poorly differentiated.

FDG-PET Scanning

Patients were instructed to fast for at least 4 hours before intravenous administration of fluorine 18–tagged FDG. The dosage of fluorine 18–tagged FDG administered was 125 μCi/kg (4.6 MBq/kg) of body weight for nondiabetic patients and 150 μCi/kg (5.6 MBq/kg) of body weight for diabetic patients. PET imaging was performed approximately 60 minutes after administration of FDG with a POSICAM.HZL mPOWER (Positron Co, Houston, Tex). No-attenuation-corrected emission scans were initially obtained in 2-dimensional, high-sensitivity mode for 4 minutes per bed position and taken from the vertical skull through to the midthighs. Immediately thereafter, a 2-bed-position attenuation-corrected examination was performed, with 6 minutes for the emission sequence and 6 minutes for the transmission sequence at each bed position. The images were usually reconstructed in a 256 × 256 matrix by using ordered subset expectation maximization corresponding to a pixel size of 4 × 4 mm, with section spacing of 2.66 mm.

PET Data Analysis

The FDG-PET data were evaluated semiquantitatively on the basis of the contrast ratio (CR) obtained as follows. The regions of interest (ROIs) were placed in the nodules and contralateral lung. Highest activities in the tumor ROI (T) and in the contralateral normal lung ROI (N) were measured. The CR was calculated by using the formula (T − N)/(T + N) in each nodule as an index of FDG uptake. After correction for radioactive decay, the ROIs were also analyzed by computing the standard uptake value (SUV), which was calculated on the basis of the following equation: Tumor activity concentration/Injected dose/Body weight. The maximum SUV within the selected ROIs was also measured and compared with the results of CR.

Statistical Analysis

All data were analyzed for significance by using the 2-tailed Student *t* test. All values in the text and tables are given as means ± SD.

TABLE 1. Tumor involvements and pathologic TNM stage for each CR value

CR of FDG uptake	Total lesions	>T1 N0 M0*	Lymphatic invasion	Vascular invasion	Pleural involvement
0.3	16	0	5	1	1
0.4	19	0	5	1	1
0.5†	22	0	5	1	1
0.6	29	2	9	2	2
0.7	37	4	14	7	6
0.8	39	4	15	8	6
0.9	43	8	19	10	8
1.0	44	8	19	10	8

*Pathologically more advanced stages than T1 N0 M0. Three of the 8 cases were p2; the other 5 were p1.
†Cutoff value of CR.

TABLE 2. PET findings and patients' characteristics, tumor size, and serum level of CEA

	CR of FDG uptake		P
	<0.5 (n = 22)	≥0.5 (n = 22)	value
Age (y, mean ± SD)	63 ± 11	64 ± 13	NS
Male (No.)	14	10	NS
Female (No.)	8	12	
Tumor size (cm, mean ± SD)	1.9 ± 0.6	2.2 ± 0.4	NS
CEA (ng/mL)			.001
<5.0	22	10	
≥5.0	0	12	

NS, Not statistically significant.

TABLE 3. Correlation between PET findings and pathologic tumor stage

		CR of FDG uptake	
Pathologic TNM	Total (n = 44)	<0.5 (n = 22)	≥0.5 (n = 22)
T1 N0 M0	36	22*	14*
T1 N1 M0	3	0	3
T2 N0 M0	3	0	3
T4 N0 M0	2	0	2

T2 is classified from pleural involvement grade, p2. T4 is classified from intrapulmonary metastasis.
*Significant difference in the frequency of T1 N0 M0 between the CR <0.5 and CR ≥0.5 groups ($P = .002$).

Results

The pathologic tumor stage was T1 N0 M0 in 36 patients and more advanced in 8 patients (ie, T1 N1 M0 in 3 patients, T2 N0 M0 in 3 patients, and T4 N0 M0 in 2 patients). Lymphatic or vascular invasion within tumors and pleural involvement was seen in 19, 10, and 8 patients, respectively. Table 1 shows the various CR values with relation to the pathologic tumor stage, lymphatic and vascular invasion, and pleural involvement. Although all adenocarcinomas with a CR of less than 0.5 were pathologically staged as T1 N0 M0, some adenocarcinomas with a CR of 0.5 or greater were more advanced than T1 N0 M0, with more frequent lymphatic and vascular invasion and pleural involvement than the former. Therefore medical records were compared between the 22 adenocarcinomas with a CR of less than 0.5 and the 22 adenocarcinomas with a CR of 0.5 or greater.

The maximum SUVs ranged from 0.5 to 3.1 (mean, 1.1 ± 0.7) in the 22 adenocarcinomas with a CR of less than 0.5 and from 1.9 to 8.5 (mean, 3.9 ± 1.8) in the 22 adenocarcinomas with CRs of 0.5 or greater, with the difference between the 2 groups being significant ($P < .001$). Two (9%) of the 22 adenocarcinomas with CRs of less than 0.5 showed an SUV of 2.5 or greater, however, both of which were pathologically staged as T1 N0 M0 and had no involvements of intratumoral vessels or pleura. Seven (32%) of the 22 adenocarcinomas with CRs of 0.5 or greater had SUVs of less than 2.5, of which 2 had a more advanced tumor stage than T1 N0 M0, 6 had lymphatic invasion, and 1 had vascular invasion.

Table 2 shows the results of PET findings with patients' characteristics, tumor size, and serum level of CEA. None of the adenocarcinomas with CRs of less than 0.5 had increased serum levels of CEA, which was significantly less frequent than the incidence of increased CEA in the 12 (55%) of 22 adenocarcinomas with CRs of 0.5 or greater ($P < .001$). There was no significant difference between the 2 groups in mean age, sex ratio, or tumor size.

Table 3 shows the correlation between PET findings and pathologic tumor stage. All adenocarcinomas (100%) with CRs of less than 0.5 were staged as T1 N0 M0. Adenocarcinomas with CRs of 0.5 or greater were staged as T1 N0 M0 in 14 (64%) patients, T1 N1 M0 in 3 patients, T2 N0 M0 caused by p2 (tumor exposure on the pleural surface) in 3 patients, and T4 N0 M0 caused by intrapulmonary metastases in 2 patients. Adenocarcinomas with CRs of less than 0.5 were more likely to be pathologic T1 N0 M0 stage than those with CRs of 0.5 or greater ($P = .002$).

Table 4 shows the correlation between PET findings and lymphatic and vascular invasion within tumors and pleural involvement. Lymphatic invasion was seen in 5 (23%) of 22 adenocarcinomas with CRs of less than 0.5, which was significantly less frequent than 14 (64%) of 22 with CRs of 0.5 or greater ($P = .006$). Vascular invasion was seen in 1 (5%) of 22 adenocarcinomas with CRs of less than 0.5, which was significantly less frequent than 9 (41%) of 22 with CRs of 0.5 or greater ($P = .004$). Pleural involvement was seen in 1 (5%) of 22 adenocarcinomas with CRs of less than 0.5, which was significantly less frequent than 7 (32%) of 22 with CRs of 0.5 or greater ($P = .02$).

Table 5 shows the correlation between PET findings and the histologic degree of differentiation. In the adenocarcinomas with CRs of less than 0.5, well-differentiated and

TABLE 4. Correlation between PET findings and tumor involvement into intratumoral vessels or pleura

Tumor involvement	CR of FDG uptake <0.5 (n = 22)	CR of FDG uptake ≥0.5 (n = 22)	P value
Lymphatic invasion			.006
Yes	5	14	
No	17	8	
Vascular invasion			.004
Yes	1	9	
No	21	13	
Pleural involvement			.02
p0	21	15	
p1-p2	1	7	

TABLE 5. Correlation between PET findings and grade of histologic differentiation of adenocarcinomas

Grade of differentiation	Total (n = 44)	CR of FDG uptake <0.5 (n = 22)	CR of FDG uptake ≥0.5 (n = 22)
Well differentiated	23	19*	4*
Moderately differentiated	17	3	14
Poorly differentiated	4	0	4

There was significant difference in frequency of well-differentiated adenocarcinomas between the CR <0.5 and CR ≥0.5 groups ($P < .001$).

TABLE 6. Correlation between PET findings and tumor stages, tumor involvement of intratumoral vessels, and tumor involvement of pleura in well-differentiated adenocarcinomas

Tumor stage and invasiveness	CR of FDG uptake >0.5 (n = 19)	CR of FDG uptake ≥0.5 (n = 4)	P value
TNM stage			<.01
T1 N0 M0	19	2	
>T1 N0 M0	0	2	
Lymphatic invasion			<.001
Yes	3	4	
No	16	0	
Vascular invasion			.02
Yes	1	2	
No	18	2	
Pleural involvement			<.01
p0	19	2	
p1-p2	0	2	

moderately differentiated adenocarcinomas were seen in 19 and 3 patients, respectively. In the adenocarcinomas with CRs of 0.5 or greater, well-differentiated, moderately differentiated, and poorly differentiated adenocarcinomas were seen in 4, 14, and 4 patients, respectively. Adenocarcinomas with CRs of less than 0.5 were more commonly well differentiated than those with CRs of 0.5 or greater ($P < .001$).

Table 6 shows the PET findings in well-differentiated adenocarcinomas with relation to the tumor stages and tumor involvements. Of the 4 well-differentiated adenocarcinomas with CRs of 0.5 or greater, each one (25%) was a pathologic T1 N1 M0 and T4 N0 M0 carcinoma, respectively; 4 (100%) had lymphatic invasion; 2 (50%) had vascular invasion; and 2 (50%) had pleural involvement. The well-differentiated adenocarcinomas with CRs of 0.5 or greater had advanced tumor stages, lymphatic and vascular invasion, and pleural involvement more frequently than those with CRs of less than 0.5 ($P < .01$, $P < .001$, $P = .02$, and $P < .01$, respectively).

Discussion

Although a criterion for diagnosing pulmonary malignancy with FDG-PET has frequently used an SUV with a cutoff value of 2.5,[20] some authors used visual evaluation, such as comparison of FDG uptake between nodules and mediastinal uptake.[21] The present study evaluated FDG uptake with CR instead of SUV for the following reasons: (1)hyperglycemia in diabetic patients decreases both the blood clearance of FDG and the accumulation of FDG in tumor tissue, and (2) SUV could be different between fat and thin patients because it is measured by using a body weight. Actually, the mean SUV of malignant pulmonary nodules has been reported to be various, ranging from 5.5 to 10.1.[22-25] In breast cancer, Wahl and coworkers[26] have demonstrated that a CR between tumor and contralateral normal breast is a reliable indicator for diagnosing malignancy. We accordingly used CR in the present study and determined that the cutoff value to differentiate between aggressive and nonaggressive adenocarcinomas was 0.5, with which we could differentiate the degree of tumor aggressiveness more accurately than with SUV.

The important points of the present study are as follows. Compared with adenocarcinomas with CRs of 0.5 or greater, those with CRs of less than 0.5 (1) did not show an increased serum level of CEA, (2) did not have lymph node metastases, (3) had less tumor involvement of vessels or pleura, and (4) were more frequently well-differentiated adenocarcinomas. The serum level of CEA in lung adenocarcinomas has been reported to be higher in N1 or N2 disease than in N0 disease.[27] FDG uptake in lung adenocarcinomas is known to often be negative in well-differentiated adenocarcinomas.[28] It has been also reported that well-differentiated adenocarcinomas are more commonly N0 stage and have less tumor involvement of vessels or pleura than moderately or poorly differentiated lesions.[9,12,13,18] Our results agree with those of these earlier studies. There were, however, 4 well-differentiated adenocarcinomas with CRs of 0.5 or greater that had more tumor aggressiveness than the 19 well-differentiated lesions with CRs of less than 0.5. We therefore consider that an FDG

uptake on PET can predict lymph node metastases and tumor invasiveness more accurately than the grade of histologic differentiation in clinical T1 N0 M0 adenocarcinomas.

Although limited resection could be a reasonable approach for T1 N0 M0 lung cancers, it has been reported that lymph node metastases are found in about 20% of clinical T1 N0 M0 adenocarcinomas.[9-11] In 1995, the Lung Cancer Study Group reported the results of a randomized control trial comparing limited resection and lobectomy for clinical T1 N0 M0 NSCLCs.[29] This trial demonstrated the inferiority of limited resection in terms of local relapse and prognosis because some patients actually had pathologic N1 or N2 disease. This is also because tumor involvement of intratumoral vessels or the pleura can cause local recurrence after limited resection, even for pathologic N0 disease, because of the spread of tumor cells into lymphatic vessels outside the primary tumor.[30] The present study showed that clinical T1 N0 M0 adenocarcinomas with CRs of less than 0.5 usually did not metastasize to the lymph nodes and seldom invaded the intratumoral vessels or pleura. This type of lung adenocarcinoma can be cured by means of limited surgical resection, such as segmentectomy or wedge resection. Although it has been reported that NSCLCs of less than 2 cm in size can be cured by means of segmentectomy with mediastinal lymph node dissection (ie, extended segmentectomy),[7] the indication of the extended segmentectomy could be expanded for adenocarcinomas with CRs of less than 0.5 that are less than 3 cm in size.

Mediastinal lymph node dissection is a useful procedure to secure complete local control of an NSCLC, with a subsequent improvement in both survival and nodal staging.[11] However, to minimize the damage caused by mediastinal node dissection in the patients with clinical stage I NSCLC, several authors reduced the dissection of some mediastinal lymph nodal stations with respect to the location of the primary tumor (ie, that the inferior and superior mediastinal lymph node stations could be reduced in the upper lobectomy and lower lobectomy, respectively).[31,32] To expand the possibility of reduction of mediastinal lymph node dissection, a successful intraoperative sentinel lymph node biopsy has been reported.[33,34] The present study showed that lymph node dissection could be reduced for clinical T1 N0 M0 adenocarcinomas with CRs of less than 0.5, without using the sentinel lymph node biopsy.

Although FDG-PET is well known to be useful for tumor staging in lung cancer, we believe that it can also predict lymph node metastases and tumor invasiveness in clinical T1 N0 M0 lung adenocarcinomas. Limited lung resection could be indicated, lymph node dissection or mediastinoscopy could be reduced, or both in this type of adenocarcinoma.

References

1. Kaneko M, Eguchi K, Ohmatsu H, et al. Peripheral lung cancer: screening and detection with low-dose spiral CT versus radiography. *Radiology*. 1996;201:798-802.
2. Yankelevitz DF, Gupta R, Zhao B, Henschke CI. Small pulmonary nodules: evaluation with repeat CT-preliminary experience. *Radiology*. 1999;212:561-6.
3. Henschke CI, Yankelevitz DF. CT screening for lung cancer. *Radiol Clin North Am*. 2000;38:487-95.
4. Nomori H, Horio H, Fuyuno G, Kobayashi R, Morinaga S, Suemasu K. Lung adenocarcinomas diagnosed by open or thoracoscopic vs. bronchoscopic biopsy. *Chest*. 1998;114:40-4.
5. Nomori H, Horio H. Colored collagen is a long-lasting point marker for small pulmonary nodules in thoracoscopic operations. *Ann Thorac Surg*. 1996;61:1070-3.
6. Nomori H, Horio H, Naruke T, Suemasu K. Fluoroscopy-assisted thoracoscopic resection of lung nodules marked with lipiodol. *Ann Thorac Surg*. 2002;74:170-3.
7. Yoshikawa K, Tsubota N, Kodama K, Ayabe H, Taki T, Mori T. Prospective study of extended segmentectomy for small lung tumors. *Ann Thorac Surg*. 2002;73:1055-9.
8. Kodama K, Doi O, Higashiyama M, Yokouchi H. Intentional limited resection for selected patients with T1 N0 M0 non-small cell lung cancer. *J Thorac Cardiovasc Surg*. 1997;114:347-53.
9. Suzuki K, Nagai K, Yoshida J, Nishimura M, Nishizaki Y. Predictors of lymph node and intrapulmonary metastasis in clinical stage IA non-small cell lung carcinoma. *Ann Thorac Surg*. 2001;72:352-6.
10. Asamura H, Nakayama H, Kondo H, Tsuchiya R, Shimosato Y, Naruke T. Lymph node involvement, recurrence, and prognosis in resected small, peripheral, non-small cell lung carcinomas: are these carcinomas candidates for video-assisted lobectomy? *J Thorac Cardiovasc Surg*. 1996;111:1125-34.
11. Naruke T, Goya T, Tsuchiya R, Suemasu K. The importance of surgery of non-small cell carcinoma of lung with mediastinal lymph node metastasis. *Ann Thorac Surg*. 1998;46:603-10.
12. Suzuki K, Asamura H, Kusumoto M, Kondo H, Tsuchiya R. Early peripheral lung cancer: prognostic significance of ground glass opacity on thin-section computed tomographic scan. *Ann Thorac Surg*. 2002; 74:1635-9.
13. Matsuguma H, Yokoi K, Anraku M, et al. Proportion of ground-glass opacity on high-resolution computed tomography in clinical T1 N0 M0 adenocarcinoma of the lung: a predictor of lymph node metastasis. *J Thorac Cardiovasc Surg*. 2002;124:278-84.
14. Higashi K, Ueda Y, Yagishita M, et al. FEG PET measurement of the proliferative potential of non-small cell lung cancer. *J Nucl Med*. 2000;41:85-92.
15. Vesselle H, Schmidt RA, Pugsley JM, et al. Lung cancer proliferation correlates with [F-18]fluorodeoxyglucose uptake by positron emission tomography. *Clin Cancer Res*. 2000;6:3837-44.
16. Ahuja V, Coleman RE, Herndon J, Patz EF. The prognostic significance of fluorodeoxyglucose positron emission tomography imaging for patients with non-small cell lung carcinoma. *Cancer*. 1998;83:918-24.
17. Vansteenkiste JF, Stroobants SG, Dupont PJ, et al. Prognostic importance of the standardized uptake value on ^{18}F-fluoro-2-deoxy-glucose-positron emission tomography in non-small cell lung cancer: an analysis of 125 cases. *J Clin Oncol*. 1999;17:3201-6.
18. Noguchi M, Morikawa A, Kawasaki M, et al. Small adenocarcinoma of the lung. Histologic characteristics and prognosis. *Cancer*. 1995; 75:2844-52.
19. Sobin LH, Wittekind Ch, editors. UICC: TNM classification of malignant tumours. 6th ed. New York: John Wiley & Sons; 2002. p. 99-103.
20. Coleman RE. PET in lung cancer. *J Nucl Med*. 1999;40:814-20.
21. Marom EM, Sarvis S, Herndon JE, et al. T1 lung cancers: sensitivity of diagnosis with fluorodeoxyglucose PET. *Radiology*. 2002;223: 453-9.
22. Dewan NA, Gupta NC, Redepenning LS, et al. Diagnostic efficacy of PET-FDG imaging in solitary pulmonary nodules. *Chest*. 1993;104: 997-1002.
23. Gupta NC, Maloof J, Gunel E. Probability of malignancy in solitary

pulmonary nodules using fluorine-18-FDG and PET. *J Nucl Med.* 1996;37:943-8.
24. Imdahl A, Jenkner S, Brink I, et al. Validation of FDG positron emission tomography for differentiation of unknown pulmonary lesions. *Eur J Cardiothorac Surg.* 2001;20:324-9.
25. Lowe VJ, Fletcher JW, Gobar L, et al. Prospective investigation of positron emission tomography in lung nodules. *J Clin Oncol.* 1998; 16:1075-84.
26. Wahl RL, Cody RL, Hutchins GD, et al. Primary and metastatic breast carcinoma: initial clinical evaluation with PET with the radiolabeled glucose analogue 2-[F-18]-fluoro-2-deoxy-D-glucose. *Radiology.* 1991;179:765-70.
27. Takamochi K, Nagai K, Yoshida J, et al. Pathologic N0 status in pulmonary adenocarcinoma is predictable by combining serum carcinoembryonic antigen level and computed tomographic findings. *J Thorac Cardiovasc Surg.* 2001;122:325-30.
28. Higashi K, Ueda Y, Seki H. F-18 FDG PET imaging is negative in bronchiolo-alveolar lung carcinoma. *J Nucl Med.* 1998;39:1016-20.
29. Ginsberg RJ, Rubinstein LV. Randomized trial of lobectomy versus limited resection for T1N0 non-small cell lung cancer. Lung Cancer Study Group. *Ann Thorac Surg.* 1995;60:615-22.
30. Ichinose Y, Yano T, Yokoyama H, Inoue T, Asoh H, Katsuda Y. The correlation between tumor size and lymphatic vessel invasion in resected peripheral stage I non-small cell lung cancer. A potential risk of limited resection. *J Thorac Cardiovasc Surg.* 1994;108:684-6.
31. Naruke T, Tsuchiya R, Kondo H, Nakayama H, Asamura H. Lymph node sampling in lung cancer: how should it be done? *Eur J Cardiothorac Surg.* 1999;16(suppl):S17-24.
32. Asamura H, Nakayama H, Kondo H, Tsuchiya R, Naruke T. Lobe-specific extent of systemic lymph node dissection for non-small cell lung carcinomas according to a retrospective study of metastases and prognosis. *J Thorac Cardiovasc Surg.* 1999;117:1102-11.
33. Liptay MJ, Masters GA, Winchester DJ, et al. Intraoperative radioisotope sentinel lymph node mapping in non-small cell lung cancer. *Ann Thorac Surg.* 2000;70:384-90.
34. Nomori H, Horio H, Naruke T, Orikasa H, Yamazaki K, Suemasu K. Use of technetium-99m tin colloid for sentinel lymph node identification in non-small cell lung cancer. *J Thorac Cardiovasc Surg.* 2002; 124:486-92.

GTS

Progression of Focal Pure Ground-Glass Opacity Detected by Low-Dose Helical Computed Tomography Screening for Lung Cancer

Ryutaro Kakinuma, MD, Hironobu Ohmatsu, MD, Masahiro Kaneko, MD, Masahiko Kusumoto, MD, Junji Yoshida, MD, Kanji Nagai, MD, Yutaka Nishiwaki, MD, Toshiaki Kobayashi, MD, Ryosuke Tsuchiya, MD, Hiroyuki Nishiyama, MD, Eisuke Matsui, MD, Kenji Eguchi, MD, and Noriyuki Moriyama, MD

Objective: To clarify the progression of focal pure ground-glass opacity (pGGO) detected by low-dose helical computed tomography (CT) screening for lung cancer.

Methods: A total of 15,938 low-dose helical CT examinations were performed in 2052 participants in the screening project, and 1566 of them were judged to have yielded abnormal findings requiring further examination. Patients with peripheral nodules exhibiting pGGO at the time of the first thin-section CT examination and confirmed histologically by thin-section CT after follow-up of more than 6 months were enrolled in the current study. Progression was classified based on the follow-up thin-section CT findings.

Results: The progression of the 8 cases was classified into 3 types: increasing size (n = 5: bronchioloalveolar carcinoma [BAC]), decreasing size and the appearance of a solid component (n = 2: BAC, n = 1; adenocarcinoma with mixed subtype [Ad], n = 1), and stable size and increasing density (n = 1: BAC). In addition, the decreasing size group was further divided into 2 subtypes: a rapid-decreasing type (Ad: n = 1) and a slow-decreasing type (BAC: n = 1). The mean period between the first thin-section CT and surgery was 18 months (range: 7–38 months). All but one of the follow-up cases of lung cancer were noninvasive whereas the remaining GGO with a solid component was minimally invasive.

Conclusions: The pGGOs of lung cancer nodules do not only increase in size or density, but may also decrease rapidly or slowly with the appearance of solid components. Close follow-up until the appearance of a solid component may be a valid option for the management of pGGO.

Key Words: ground-glass opacity, low-dose helical computed tomography screening, lung cancer

(*J Comput Assist Tomogr* 2004;28:17–23)

Focal pure ground-glass opacities (pGGOs), or nodules of the lungs, has become a major concern as low-dose helical computed tomography (CT) screening for lung cancer becomes more widely available, not only in the field of diagnostic imaging,[1–5] but also in the field of limited surgery.[6–10] GGO is a finding on thin-section CT images of the lung which has been described as a hazy, increased attenuation of the lung tissue with preservation of the bronchial and vascular margins. GGO is usually a nonspecific finding that is found in many types of pulmonary disease.[11] However, some investigators have recently reported that most localized pGGOs or focal GGOs are malignant.[1,2,5] Although a few reports have described the evolution of lung cancer using conventional chest CT,[12–14] thin-section CT[15–17] and low-dose screening CT,[18,19] the natural history of peripheral lung cancers that exhibit as pGGO on thin-section CT images detected using low-dose helical CT screening is still unclear.

The purpose of this retrospective study was to clarify the progression of pGGOs, which were not visible on chest radiographs, detected by low-dose helical CT screening examinations performed every 6 months. We evaluated the progression of pGGOs based on the thin-section CT findings obtained during the follow-up after the first thin-section CT.

PATIENTS AND METHODS

Subjects

Between September 1993 and January 2003, low-dose helical CT screening was conducted semiannually in Tokyo by

From the Division of Thoracic Oncology (Drs Kakinuma, Ohmatsu, Yoshida, Nagai, and Nishiwaki), National Cancer Center Hospital East, Tsukiji, Chiba Japan; the Divisions of Endoscopy (Drs Kaneko and Kobayashi), Diagnostic Radiology (Drs Kusumoto and Moriyama), and Thoracic Surgery (Dr Tsuchiya), National Cancer Center Hospital; the Division of Thoracic Surgery (Dr Nishiyama), Social Health Insurance Medical Center, Okubo, Japan; (Dr Matsui); the Anti–Lung Cancer Association, Ichigaya, Japan; and the Division of Internal Medicine (Dr Eguchi), School of Medicine, Tokai University, Isehara, Japan.

This study was supported in part by a Grant-in-Aid for Cancer Research (13-8) from the Ministry of Health, Labor, and Welfare of Japan and by a Grant-in-Aid from the Second-Term Comprehensive 10-Year Strategy for Cancer Control.

Reprints: Ryutaro Kakinuma, MD, National Cancer Center Hospital East, 6-5-1 Kashiwa-no-ha, Kashiwa, Chiba 277-8577, Japan (e-mail: rkaki@east.ncc.go.jp).